How urban surfaces impact severe thunderstorms:

modelling the impact of the city of Berlin on a case of heavy precipitation

MSc. Thesis Meteorology and Air Quality

Max Verhagen

Wageningen University, Wageningen, The Netherlands

January, 2014

How urban surfaces impact severe thunderstorms:

modelling the impact of the city of Berlin on a case of heavy precipitation

M.T.T. Verhagen

880512874020

Supervisors

R. J. Ronda and G. J. Steeneveld

Preface

During my internship, I investigated the possibility to improve the radar projection. This project sparked my interest to investigate the impact of a city on a severe thunderstorm. For my research, I preferred a large city in the Netherlands, but this was discouraged because of the strong influence of the sea breeze. The choice of Berlin is interesting, because Berlin is a city with a high urban vegetation cover and is located in a relatively flat landscape. These conditions are perfect for my study. Due to the resulting enthusiasm after the first WRF results, I performed many model runs to study the urban precipitation effect in Berlin.

Abstract

Severe thunderstorms can cause problems in urban areas. Heavy precipitation has to be drained away, often by undersized or even damaged sewer pipes. This can result in flooding and damages in an urban area. Despite its importance, there is a lack of knowledge on the impact of urban areas on severe thunderstorms. There are three main mechanisms which can cause urban precipitation disturbances: (I) low-level mechanical turbulence through urban obstructions to the airflow; (II) the addition of sensible heat flux from the urban area; (III) the urban (anthropogenic) aerosols. The effects of mechanism (III) have not been investigated in this study.

This WRF model study investigated the situation with a severe thunderstorm in the area of Berlin on September 11, 2011. In seven cases, a different feature of the urban area is examined with regard to the impact of an urban area on the severe thunderstorm.

The study suggests approximately 0.5–4.0 [℃] higher urban temperatures and approximately 2.0 percent less to 14.7 percent more urban precipitation in and downwind of the urban area, compared to the rural temperature and precipitation. The result indicates a decreased latent heat flux and increased sensible heat flux in the urban area, which correspond to mechanism (II). The cases urban vegetation cover and city size results correspond to mechanism (II). The anthropogenic heat causes higher CAPE values, which results in a destabilized effect of the urban boundary layer (mechanism (I)). This results in more precipitation in the urban area as the anthropogenic heat increases. The results of the albedo and building height correspond to mechanism (I) as well.

Keywords: Urban heat island, Precipitation, City sizes, Anthropogenic heat, Urban vegetation fraction, WRF.

Table of Contents

1   Introduction

1.1   Theoretical background

The assumption that thunderstorms always pass around an urban area is a well-known saying. However, is there any truth in this saying? To answer this question, several studies have investigated the impact of urban areas on severe thunderstorms. This investigation differs from previous research. This research has been focused on the impact of several urban features on a severe thunderstorm, instead of one specific urban feature per research.

The research is relevant because of the increasingly expensive damages in urban areas, caused by thunderstorms. Currently, over 3.3 billion people live in urban areas. Next to this, the urban area is increasing rapidly. According to Stepherds & Burian (2003) and the United Nations Population Fund (2007), the number of people living in urban areas will increase up to 5 billion (60 percent) in 2030.

However, severe thunderstorms have significant impact on city dwellers and the economy. The storms cause problems for sewer systems in an urban area. Due to the impervious surface, rainwater cannot infiltrate into the ground. As a result, the precipitation has to be drained by the sewage system. This can result in urban flooding, flooded basements and infrastructure damages in case of high rain intensity, caused by undersized or damaged sewer pipes. According to the IPCC-4 report, global warming increases the frequency of severe precipitation events (Willems et al., 2012; Wan & Zhong, 2013). Therefore, it is necessary to assess the impact of urbanisations on convective precipitation properly. Especially since severe convective precipitation can cause problems in short time periods, in contrast to stratiform precipitation which has been ignored in this study.

The urban heat island (UHI) is the phenomenon in which the average temperature of an urban area is higher than the surrounding (rural) area. This effect is caused by differences in albedo, surface roughness, evapotranspiration and energy flux (Lin et al., 2011). As a result, the energy and radiation balances in rural and urban areas differ (Oke, 2006). The radiation and energy balance are respectively:

$$Q^* = (1 - \alpha) \cdot S^{\downarrow} + \varepsilon \cdot L^{\downarrow} - \varepsilon \cdot \sigma \cdot (T_{skin})^4 \qquad [1]$$

$$Q^* + H_A = H_S + L_v E + G \qquad [2]$$

where Q^* is the net radiation, α is the albedo, $S^{\downarrow}$ is the incoming shortwave radiation [W/m^2], ε is the emissivity, $L^{\downarrow}$ is the incoming longwave radiation [W/m^2], σ is the Stefan-Boltzmann constant (5.67·10^{-8} [W/m^2]) and T$_{skin}$ is the skin temperature [K]. The H$_A$ is the anthropogenic

heat production in equation [2], H_S the sensible heat flux, L_vE the latent heat flux and G the soil flux [W/m²].

In rural areas the energy balance is driven by the shortwave (daytime) and longwave (night-time) radiation, the sensible and latent heat fluxes and the soil flux. The heat exchange is determined by the surface characteristics (type of vegetation or moisture content), the thermal properties of the soil and the level of turbulence in the atmosphere (Oke, 1982). In urban areas, the energy and radiation balances differ from rural areas due to the high heat capacity of urban materials, and increased incoming radiation caused by multi-reflection and absorption. Therefore, the surface albedo, convective available potential energy (CAPE) and evapotranspiration decreases, deepens the boundary layer, and increases the surface temperature in an urban area (Zhang et al., 2009; Yang et al., 2014). Furthermore, the urban albedo is 0.05 to 0.1 lower and results in more net solar radiation (Christen and Vogt, 2004). There is a heat accumulation during daytime and a release of heat at night in the urban areas (Oke, 1982).

Another release is the anthropogenic emission of polluted particles. The urban heat island and pollution (aerosols) are related to precipitation processes (Wan & Zhong, 2013). In several studies, large-scale urbanisation has a significant effect on temperature, precipitation and deterioration of visibility in the area near Shanghai (Wan et al., 2012; Wan & Zhong, 2013).

The urban energy balance and urban pollution can influence the precipitation pattern in and around urban areas. According to Guo & Wang (2006), an increase in severe precipitation events has already been observed in urban areas. According to Changnon et al. (1990), the urban areas have 5 to 10 percent more cloud cover and 13 to 15 percent more precipitation than the neighbouring rural areas. The research of METROMEX shows an increase of 5 to 25 percent of precipitation within 50 to 75 kilometres downwind of several American cities during the summer months (Changnon et al., 1981; Wan & Zhong, 2013). Another result shows that changes in urban precipitation depend on the degree of urbanization (Miao et al., 2010). According to Wan & Zhong (2013), the precipitation in the urban area decreased. There are three main mechanisms which can cause urban precipitation disturbances (Huff & Changnon, 1973; Oke, 1982; Jauregui & Romales, 1996; Miao et al., 2009; Yang et al., 2014):

I.   Low-level mechanical turbulence through urban obstructions to the airflow;
II. The addition of sensible heat flux from the urban area;
III. The urban (anthropogenic) aerosols.

Mechanism I: low-level mechanical turbulence

The airflow changes due to the increased roughness length of the urban area and the urban heat island effect. The increase in the sensible heat flux and roughness length can destabilize the urban boundary layer and can enhance the precipitation (Stepherd & Burian, 2003). The low-level convergence and the convection have been strengthened in this situation (Collier, 2006; Guo & Wang, 2006). Especially on the leeward side of a city, the surface convergence is enhanced (Huff & Changnon, 1973). As a result, rainfall has often been intensified during moderately heavy rain situations (Chagnon et al., 1990).

Mechanism II: addition of sensible heat flux

The sensible heat flux increases in an urban area and as a consequence the latent heat flux decreases, both compared to rural areas. The urban soil moisture content and the precipitation convective clouds decreases (Bornstein, 1968; Guo & Wang 2006; Matheson & Ashie, 2008). However, the sensible heat has a larger effect in determining the location of (convective) clouds than soil moisture content. The warmer and relatively dry urban soils possibly inhibit the transportation of moisture in the urban boundary layer. This results in a decrease of the latent heat flux, convective available potential energy and precipitation (Wan & Zhong, 2013).

Mechanism III: urban aerosols

The aerosols can affect the radiative forcing (direct effect). Aerosols scatter and absorb solar radiation; reemit longwave radiation back to the surface and have effect on the surface temperature (Ramanathan et al., 2001). Another interaction is the aerosol-cloud interaction. The aerosols change the stability of the atmosphere due to heating (sensible heat flux increase) and affect the evaporation of the clouds (Hansen et al., 1997; Jin et al., 2005). The anthropogenic aerosols in urban areas can suppress, invigorate or suppress and invigorate the convection and low-level convergence (Schmid, 2013). There is slightly more evidence of the dynamic modification processes than microphysical modification processes (Huff & Changnon, 1973).

Explaining the relation between urban areas and precipitation is and will be very difficult. Precipitation is affected by different factors and the raindrops do not fall perpendicularly through wind direction and wind speed (Kondo, 2012). The results can be caused by model errors as well (Seino & Aoyagi, 2012; Wan et al., 2012). The anthropogenic heat in urban heat island is not included in current models either (Matheson & Ashie, 2008).

Therefore it is necessary to investigate the impact of an urban area on convective precipitation for different cities around the world (Guo & Wang, 2006). The *aim* of this study is to understand the physical mechanisms of the urban impacts on regional (convective)

precipitation. We have selected a severe thunderstorm situation in western Europe on September 11, 2011 to investigate the impact of urban area and urban features on convective precipitation (Chapter 2.2).

1.2   Research Question

This WRF study investigated the 'urban meteorological effect' on convective precipitation. For this study, two research questions are formulated:

1) *Could WRF reproduce the squall line for the situation of September 11, 2011 in the area of Berlin?*

2) *What is the impact of urban features on convective precipitation?*

The research investigates seven cases to answer the research questions:

- Case 1: Reference Run, representing the selected day;
- Case 2: Run without Berlin in the model;
- Case 3: Run with different city sizes;
- Case 4: Run with various anthropogenic heat;
- Case 5: Run with various building heights;
- Case 6: Run with various building albedo's;
- Case 7: Run with different vegetation covers within Berlin;

Various studies have shown the plausible effect that urban areas affects the convective precipitation. However, there is still a lack of knowledge on the physical mechanisms and impacts. According to Tayanç et al. (1997), there is no evidence that an urban area affects the precipitation. These contradicting results indicate that the results are not unanimously, and tend to a city and variable dependency. Therefore, an analyse of seven different features of an urban area have been investigated to answer the two research questions. Each case investigated a different feature of the city and its impact on the severe thunderstorm. The cases have been described in more detail in the Methodology (Chapter 2.3).

This study goes beyond previous research, because of the investigation of the impact of various urban features instead of one urban feature on convective precipitation, and partly because of unique cases (4 and 7) which are not investigated in European cities yet.

Several cases have been covered in order to answer the two research questions in the MSc thesis. The thesis is organized as follows. Chapter 2 contains the description of the used method and model runs. The results of cases 1 to 7 are presented in chapter 3, followed by the discussion and conclusion in chapter 4 and 5 respectively.
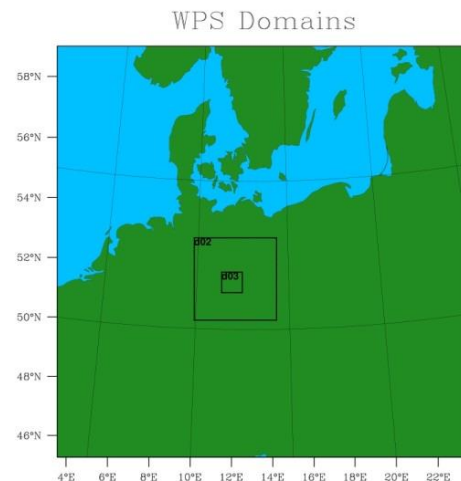
2   Methodology

2.1   Model domain and initialisation

The Weather Research and Forecasting (WRF version 3.5) model is used in this study to simulate the impacts of an urban feature on convective precipitation (Skamarock et al., 2008). The WRF model is a suitable tool because WRF is applied frequently for short and medium range weather forecasts (Yair et al., 2010). Moreover, the WRF model has often been used for urban precipitation modelling, for example in Miao et al. (2010) and Lin et al. (2011).

In this study we use three nested domains, which plotted in figure 1. Based on literature (e.g. Theeuwes et al., 2013), the largest domain of WRF is domain 1 (D01) with a horizontal grid spacing of 25 kilometres and 61x61 grid cells. The mother domain includes many countries in the western and central Europe with the central point in Berlin (52.515N, 13.407E).

The selected area is designed to capture the synoptic features. The first domain (D02) had a horizontal grid spacing of 5 kilometres and 61x61 grid cells. The innermost domain (D03) covered the area of Berlin and had a horizontal grid spacing of 1 kilometre with 100x100 grid cells.

The vertical structure of the WRF model consists of 35 eta layers that cover the entire troposphere. An adaptive time step is employed, in the outer domain 120 seconds and decreases with a ratio of 5 in each domain.

Figure 1. *The three domains in the WRF model, the mid-point is Berlin.*

2.2   Case description

The urban area of Berlin has been investigated, because the city is located relatively far (>150 [km]) from the sea, in order to prevent the influence of a sea breeze (based on Theeuwes et al., 2013). In addition, Berlin is located in a relatively flat area of Germany, in order to prevent influences of the topography. According to e.g. Li et al. (2011) and Yang et al. (2014), severe thunderstorms are more influenced by urban features than light showers. Eventually, the weather condition of September 11, 2011 has been selected.

On 11 September 2011, heavy showers with lightning and hail caused severe damage in central and the eastern part of Germany. The inhabitants in the area between Magdeburg and Halle reported a tornado. Many roads were flooded due to heavy rainfall and there were

several power failures. The resulting damage was estimated to a few million euros and even one person died trough a flying tile ("Heftiger Regen überflutet Autobahn", 2011 and "Unwitter 11.9.2011", 2011).

Figure 2a shows the weather map of Europe on September 11, 2011. A high pressure area in southeast Europe transported very warm and moist air to the western and central part of Europe. The warm air mass had a temperature of 20 [°C] at 850 [hPa] height (1500 metres height), which indicates a very warm air type. The dewpoint was on average 20 [°C]. This resulted in a night-time minimum temperature of 20 [°C], while the surface temperature reached values of 30 [°C] or more during daytime. On the west side of the very warm air, a cold front has been located with the possibility of heavy thunderstorms.

Figure 2. a) The weather map of 11 September 2011 with the two depressions across the Atlantic Ocean and the large high pressure system over the European continent. The cold front (indicated by the arrow) is above Germany at 12 UTC. b) Two F1 tornadoes were confirmed, this one in Elsnigk (Sachsen-Anhalt) close to Berlin.

The heavy showers with lightning and hail are the result of very unstable conditions in Germany. In the days before September 11, the low pressure system with a core pressure of 975 hPa stagnated north of Ireland. In the meantime, old hurricane Katia with a core pressure of 969 hPa moved towards the Netherlands and Belgium (figure 2a). The cold front moved eastwards. During the night of 10 to 11 September, this situation caused lightning in the Netherlands and in northwest Germany. During the morning on September 11, the first thunderstorms developed rapidly over the western part of Germany, in which the convective available potential energy (CAPE) reached values above 1.0 [kJ/kg] and a large vertical wind shear. These are ideal conditions for the development of severe supercells. Large areas in Germany were confronted with heavy rainfall and hail with diameters of 5 centimetres. As a consequence, several facades and cars were badly damaged and basements were flooded. Moreover, the heavy water- and mudflows caused a closure of Motorway 14 (near Berlin). The thunderstorms not only caused heavy rains, strong winds (>100 [km/h]) were measured as well in central Germany ("Heftige Gewitter", 2011).

2.3   Model configuration and experimental design

2.3.1 Reference Run (Case 1)

To determine the best reference run, several schemes for the numerical and physical processes have been validated. An overview of the schemes is illustrated in table 1. There are several schemes available in the WRF model. To select the best schemes for the seven cases, a sensitivity analysis has been perform for the Microphysics, Planetary Boundary Layer, Cumulus Parameterization and Land Surface scheme. The selected schemes for the Short- and Longwave Radiation and Surface Layer were fixed during the reference run, respectively the Dudhia scheme (Dudhia, 1989), RRTM scheme (Mlawer et al., 1997) and the Janjic scheme (Janjic, 2002).

Table 1. *An overview of the used schemes for the reference run (case 1). The first three schemes are fixed, the other schemes have been investigated in case 1.*

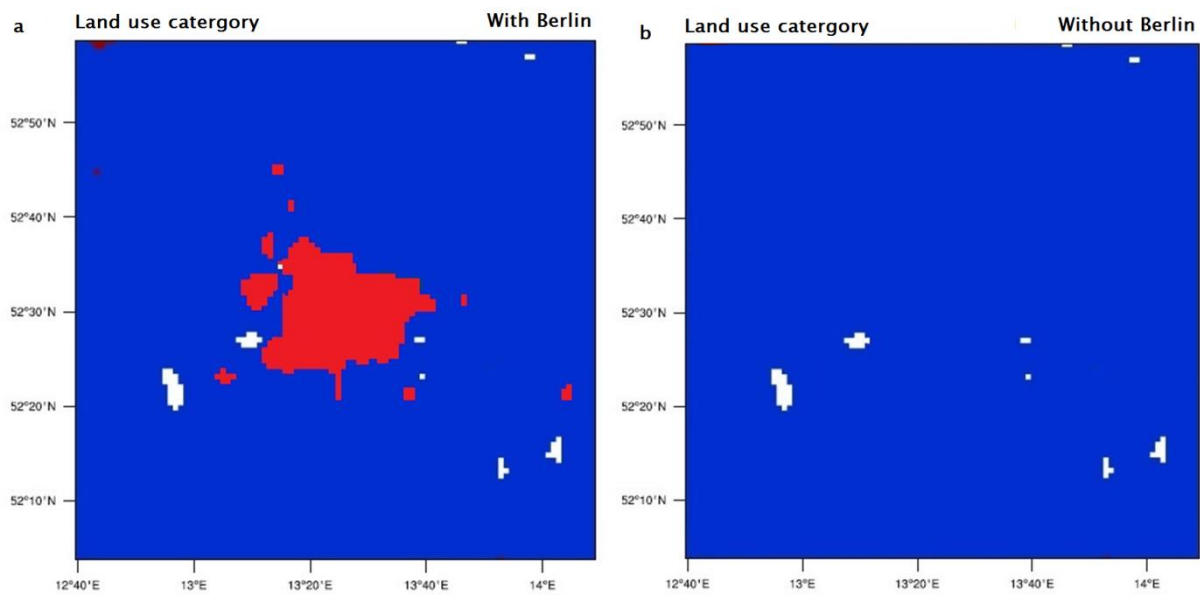| Numerical and physics process	Schemes and model
Shortwave Radiation	Dudhia
Longwave Radiation	RRTM
Surface Layer	Janjic
Microphysics	·Ferrier (new Eta) ·WSM6
Planetary Boundary Layer	·Yonsei University ·Mellor-Yamada-Janjic
Cumulus Parameterization	·Kain-Fritsch ·New Simplified Arakawa-Schubert
Land Surface	·Noah Land Surface Model ·5-layer thermal diffusion

Two Microphysics schemes have been simulated for the reference run: the Ferrier (new Eta) and the WSM6 schemes (Hong & Lim, 2006; Rogers et al., 2008). The WSM6 scheme is similar to the Ferrier scheme, the only difference is the modification of the WSM6 scheme for tropical conditions. The Yonsei University (YSU) scheme and the Mellor-Yamada-Janjic (MYJ) scheme have been simulated. This is a comparison between a non-local scheme and an eta implementation of a 1.5-order local closure scheme respectively (Mellor & Yamada, 1982; Janjic, 2002; Hong et al., 2006). According to Pagowski (2004), the YSU scheme underestimated the heat transfer between the surface and atmosphere. However, the MYJ scheme underestimated the heat transfer even more. The Kain-Fritsch scheme and the New Simplified Arakawa-Schubert scheme have been selected for the Cumulus Parameterization. The New Simplified Arakawa-Schubert scheme uses a simple mass-flux scheme with a shallow mixing scheme, while the Kain-Fritsch scheme uses a deep and shallow convection subgrid scheme for the WRF simulations (Kain & Fritsch, 1993; Han & Pan, 2011). The 5-layer thermal diffusion scheme in the Land Surface physics uses five soil layer temperatures,

while the Noah Land Surface uses the temperatures and moisture content of four soil layers (Dudhia, 1996; Ek et al., 2003).

Next, the temperature and precipitation outputs have been compared and validated with the observation of Berlin's four weather stations (data from *Wunderground*). The four weather stations were IBERLINB13 (southeast Berlin), IBERLINB15 (southwest Berlin), IBERLINB24 (east Berlin) and MAR542 (north Berlin). The station MAR 542 is the weather station located at the Berlin Tegel airport. The observations of the remaining three weather stations have been used for the validation after a careful selection of 13 amateur weather stations (e.g. data completeness) in the urban area of Berlin. The radar- and sounding model outputs have been validated with the radar (figures from *Niederschlagradar*) and the sounding of Lindenberg (figures from *University of Wyoming*).

2.3.2 Urban versus nonurban (Case 2)
In this case we compared the model run with the Berlin and the model run without the city Berlin. The urban area land use category (LU=1, red colour) has been replaced by the land use category dryland, cropland and pasture (LU=2, blue colour) (figure 3). In this case, the effects of 'original' Berlin has been simulated on the severe thunderstorm.

Figure 3. Land use in domain 3 for the model runs a) with the city Berlin (red area) and b) without the city.

2.3.3 Influence city size on convective precipitation (Case 3)

For case 3 to case 7, the 'original' Berlin was replaced by an idealized circular city in the WRF model. The 'new' circular city Berlin had different sizes (figure 22, Annex), namely:

- 10 kilometres diameter, comparable to The Hague;
- 20 kilometres diameter, comparable to the downtown of Berlin;
- 50 kilometres diameter, comparable to London and Paris;
- 75 kilometres diameter, very big city;
- 100 kilometres diameter, very big city.

This case investigated the impact of city sizes on a severe thunderstorm.

2.3.4 Influence anthropogenic heat on the severe thunderstorm (Case 4)

Case 4 investigated different anthropogenic heats in the urban area. According to Bohnenstengel et al. (2013), the anthropogenic heat flux has a smaller positive effect on temperatures in the urban areas during the summer period than in the winter period. Several values of anthropogenic heat have been investigated. According to Matheson & Ashie (2008), the maximum value of the anthropogenic heat flux is 32 to 107 [W/m^2]. We selected a very small anthropogenic heat with a maximum anthropogenic heat value of 2 [W/m^2], an anthropogenic heat maximum on a summer day (40 [W/m^2]) and a very high maximum anthropogenic heat flux of 100 [W/m^2] in the urban area. The Large scale Urban Consumption of energY (LUCY) model created a realistic daily cycle of the anthropogenic heat (Allen et al., 2011). LUCY calculated an anthropogenic heat in the urban area of Berlin of 40 [W/m^2] on September 11, 2011.

2.3.5 Building height in the urban area (Case 5)

The model run has simulated various buildings heights in this case. The building heights in an urban area can affect the urban energy balance and turbulent fluxes. The buildings in the urban area can produce a barrier effect as well, resulting in a possible flow around the urban area (Lin, 2000). In this study, we have investigated three values of building heights in the idealized circular city, namely 1.5 metres, 7.5 metres and 15 metres. The low heights have been selected due to a low maximum building height policy (22 metres) in the city centre of Berlin since 1991 ("Het nieuwe Berlijn wordt normaal", 1995).

2.3.6 Albedo in urban areas (Case 6)

This case investigated different albedos in the urban area. The albedo is very heterogeneous in an urban area due to the different albedos of roads, roofs, walls and parks. Urban albedos are typically in the range 0.10 to 0.20 [−], but in some African cities the albedo is even higher (Taha, 1997). The albedo in urban canyons is 0.14 [−], for individual facades 0.20 [−] and for grass 0.19 [−]. According to Taha (1997), the high albedo reduces the amount of absorbed solar radiation and cools the surfaces. In this case four urban albedos have been modelled: a model run with a low albedo (0.10 [−]) and a run with a high albedo (0.30 [−]).

The third model run uses an albedo of 0.15 [-]; the fourth model run uses an albedo of 0.20 [-]. These two albedo values have been selected on the basis of the previous albedo values.

2.3.7 Vegetation cover in urban area (Case 7)

Case 7, so-called 'vegetation cover in the urban area', were seven model runs with different vegetation covers (LU = 5, cropland/grassland mosaic) within the urban area of Berlin. According to the website of Fachvereinigung BauwerksBegrünung (FBB), 25 percent of the roofs in Berlin are roof gardens. There are several large parks in Berlin as well, for example the 'Tiergarten', 'Volkspark Hasenheide' and the 'Spreepark Berlin'. The influence of the seven different urban vegetation covers has been investigated on the severe thunderstorm. The vegetation covers are 1, 10, 20, 30, 40, 50 and 100 percent of the urban area.

The following aspects of different city sizes have been investigated in this seven cases and compared with the run without Berlin: the (dewpoint) temperature, precipitation, relative humidity, CAPE, latent heat flux, sensible heat flux, vertical wind speed and convergence. The vertical wind speed and precipitation in the urban area and in the urban downwind area has been investigated in more detail in several cases. For the vertical wind speed, the selected square area was between 13°25'E-14°05'E and 52°30'N-52°55'N in domain 3 (about 160 measuring points). The selected square area for the precipitation was between 13°30'E-15°20'E and 52°30'N-53°45'N in domain 2 (about 250 measuring points).

2.4   Datasets

For all WRF model runs, the dataset of the ECMWF has been used. The ECMWF dataset has been a 6 hourly operational analysis with a resolution of 0.5° as boundary and initial conditions. The first part of the model run had a duration of 60 hours (from September 8, 2011 0.00 UTC to September 11, 2011 12.00 UTC). This part of the model run has only been used as a spin-up run for the idealized circular city in the WRF model and has not been used in the further analysis. The simulation time of the second part of the model run had a duration of 30 hours (from September 11, 2011 12.00 UTC to September 12, 2011 18.00 UTC). The last time step of the urban road-, roof- and wall temperatures (in URBPARM.TBL) from the first part of the model run have been used as initial urban road-, roof- and wall temperatures for the second part of the model run. This method has been selected in order to avoid too cool urban surfaces.

2.5   Evaluation methodology

The approach whereby the model results are compared with the observed values was used. It was important that the output of the reference run was very similar to the observed temperature and precipitation. The research used the mean bias error (MBE), root mean square error (RMSE), mean absolute error (MAE) and the correlation (CC) in order to validate

the modelled and observed temperature and precipitation. The following formulas have been used (Willmott, 1982):

$$MBE = \frac{1}{N}\sum_{i=1}^{N}(P_i - O_i) \qquad [3]$$

$$RMSE = \sqrt{\frac{1}{N}\sum_{i=1}^{N}(P_i - O_i)^2} \qquad [4]$$

$$MAE = \frac{1}{N}\sum_{i=1}^{N}|(P_i - O_i)| \qquad [5]$$

Here N is the number of cases (N=48), P_i is the value of the model and O_i is the observed value (Willmott, 1982). This is calculated for both the temperature and precipitation of the four Berlin's weather stations IBERLINB13, IBERLINB15, IBERLINB24 and MAR542 (figure 21, Annex).

3 Results

3.1 Reference Run

3.1.1 Parameterization

This case is the reference run of the situation on September 11, 2011. First the sensitivity of the model outcome to the selected start time of the reference runs has been analysed. An increased spin-up time of the WRF model resulted in a deteriorated reproduction of the convective conditions. Next, the physics and dynamical options has been investigated. Two different schemes of the Microphysics, Cumulus Parameterization, Land Surface and Planetary Boundary Layer have been simulated with the sensitivity analysis and validated with four temperature and precipitation observations in the area of Berlin. Figure 21 (Annex) illustrates the four weather stations in Berlin. For case 2 to case 7, the optimal scheme combination have been used.
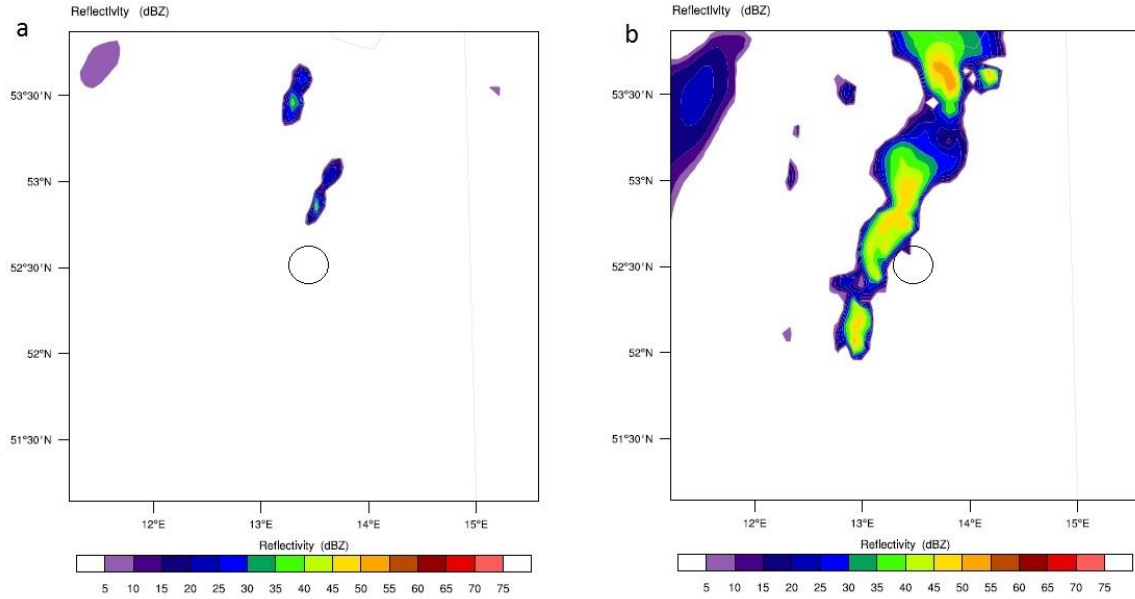
Finally, the reflectivity of the modelled and observed precipitation intensity, radio sounding, temperature and precipitation amounts has been validated.

3.1.2 Model start time

The runs started on 8 September 2011 00:00 UTC and finished at 12 September 2011 18:00 UTC. We proved that the start time of a model run has been an important factor in the reproduction of the intensity and location of the squall line. Several runs with different start times have been studied for the optimal reproduction of the squall line. The following start times were validated:

- September 8, 2011 00.00 UTC
- September 9, 2011 12.00 UTC;
- September, 10 2011 12.00 UTC;
- September, 11 2011 00.00 UTC;
- September, 11 2011 06.00 UTC;
- September, 11 2011 12.00 UTC.

The squall line has been located too far to the north of the domain compared to the actual situation for the model runs with a start time on 8, 9 and 10 September 2011. For the three above-mentioned start times, the intensity of the precipitation was too low compared to the actual situation as well (figure 4a). The model runs with start time on September 11, 2011 12.00 UTC showed the optimal reproduction of the actual situation (figure 4b). The squall line passed the urban area of Berlin. Thus we decided to proceed with this starting time for the optimal precipitation intensities of the modelled squall line compared to the actual situation by using the optimal combination of the physics and dynamical options.

Figure 4. *The modelled radar reflectivity on September 11, 2011 18.00 UTC for a) the area of Berlin with the model start time on September 11, 2011 00.00 UTC (domain 2), and b) the radar reflectivity with start time September 11, 2011 12.00 UTC (domain 2).*

3.1.3 Physics and dynamical options

The model results for the selected physics and dynamical options have been validated with the observations of Wunderground. One of the requirements was that the simulated squall line had its track over the city Berlin. This was a problem in many model runs. As mentioned previously, the squall line was located too northern in the domains between 18.00 and 19.00 UTC. Four model runs fitted the requirements, namely:

- Run FER_NOAH_MYJ_KF;
- Run FER_5LTD_MYJ_KF;
- Run WSM6_NOAH_MYJ_KF;
- Run WSM6_5LTD_MYJ_KF.

Runs *FER_NOAH_MYJ_KF* and *FER_5LTD_MYJ_KF* had the Ferrier (new Eta) scheme and runs *WSM6_NOAH_MYJ_KF* and *WSM6_5LTD_MYJ_KF* had the WSM6 scheme for the Micro Physics. In addition, run *FER_NOAH_MYJ_KF* and *WSM6_NOAH_MYJ_KF* had the Noah LSM and runs *FER_5LTD_MYJ_KF* and *WSM6_5LTD_MYJ_KF* had the 5-layer thermal diffusion scheme for the Land Surface. The Planetary Boundary Layer and Cumulus Parameter Parameterization were for the four model runs the same, namely the Mellor–Yamada–Janjic scheme and the Kain–Fritsch scheme respectively. The mean bias error (MBE), root mean square error (RMSE), mean absolute error (MAE) and the correlation (CC) have been used. The result of the validation analysis is shown in table 2.

14

Table 2. The validation of the selected model runs for temperature and precipitation.

Temperature	MBE [K]	RMSE [K]	MAE [K]	CC [−]
Run FER_NOAH_MYJ_KF	0.83	1.67	1.03	0.95
Run FER_5LTD_MYJ_KF	0.84	1.69	1.01	0.94
Run WSM6_NOAH_MYJ_KF	0.55	1.22	0.74	0.97
Run WSM6_5LTD_MYJ_KF	0.60	1.33	0.82	0.96

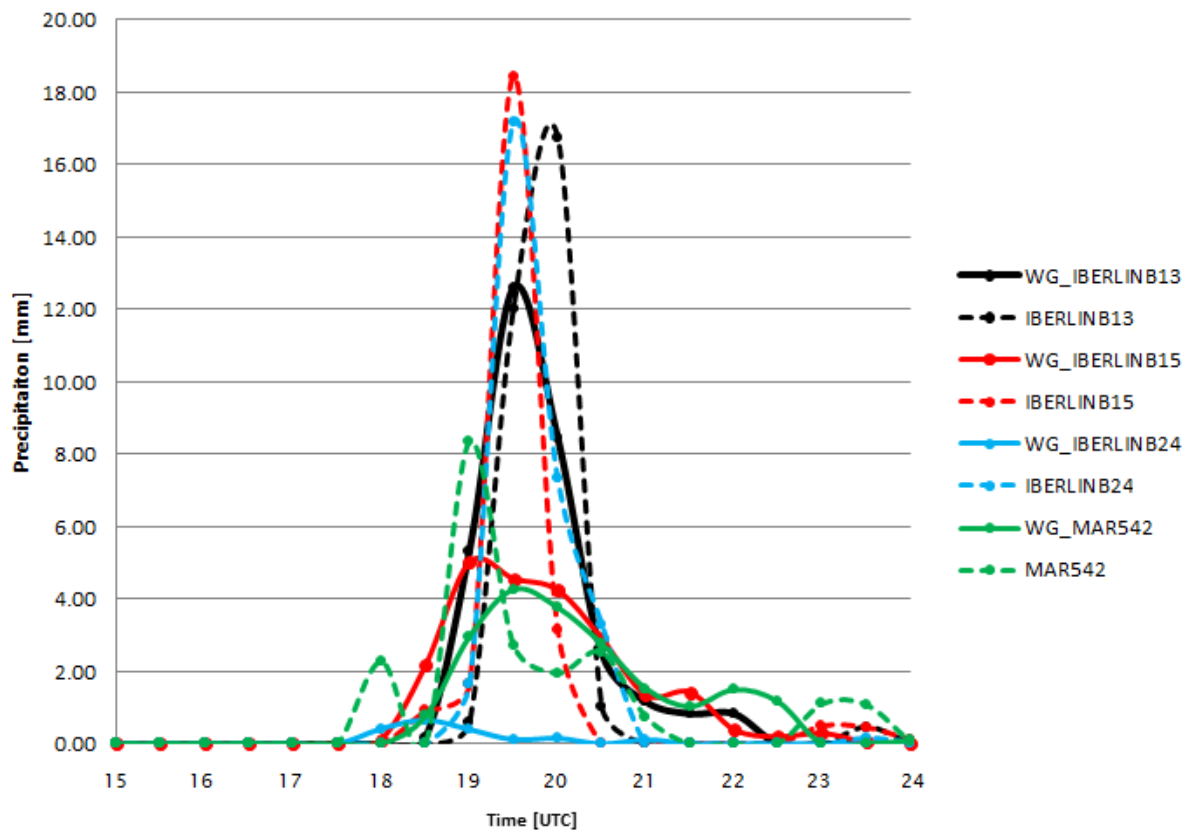| Precipitation	MBE [mm]	RMSE [mm]	MAE [mm]	CC [−]
Run FER_NOAH_MYJ_KF	0.02	1.58	0.53	0.37
Run FER_5LTD_MYJ_KF	−0.04	1.39	0.47	0.35
Run WSM6_NOAH_MYJ_KF	0.16	1.82	0.49	0.55
Run WSM6_5LTD_MYJ_KF	0.32	2.09	0.60	0.56

The focus has been on the RMSE, MAE and the correlation between the modelled and observed values of the temperature and precipitation. Table 2 shows that the RMSE of runs *FER_NOAH_MYJ_KF* and *FER_5LTD_MYJ_KF* for temperature had higher values and for precipitation slightly lower values than runs *WSM6_NOAH_MYJ_KF* and *WSM6_5LTD_MYJ_KF*. The correlation of runs *FER_NOAH_MYJ_KF* and *FER_5LTD_MYJ_KF* for temperature and precipitation had lower values than runs *WSM6_NOAH_MYJ_KF* and *WSM6_5LTD_MYJ_KF*. Finally, run *WSM6_NOAH_MYJ_KF* has been selected as optimal combination and this model run has been used for the further cases. An overview of the selected physics and dynamical options of run *WSM6_NOAH_MYJ_KF* has been shown in table 3. The precipitation, radar and soundings have been investigated in the final step of the verification.

Table 3. An overview of the settings of the physics options for the reference run, which has been used in case 2 to case 7.

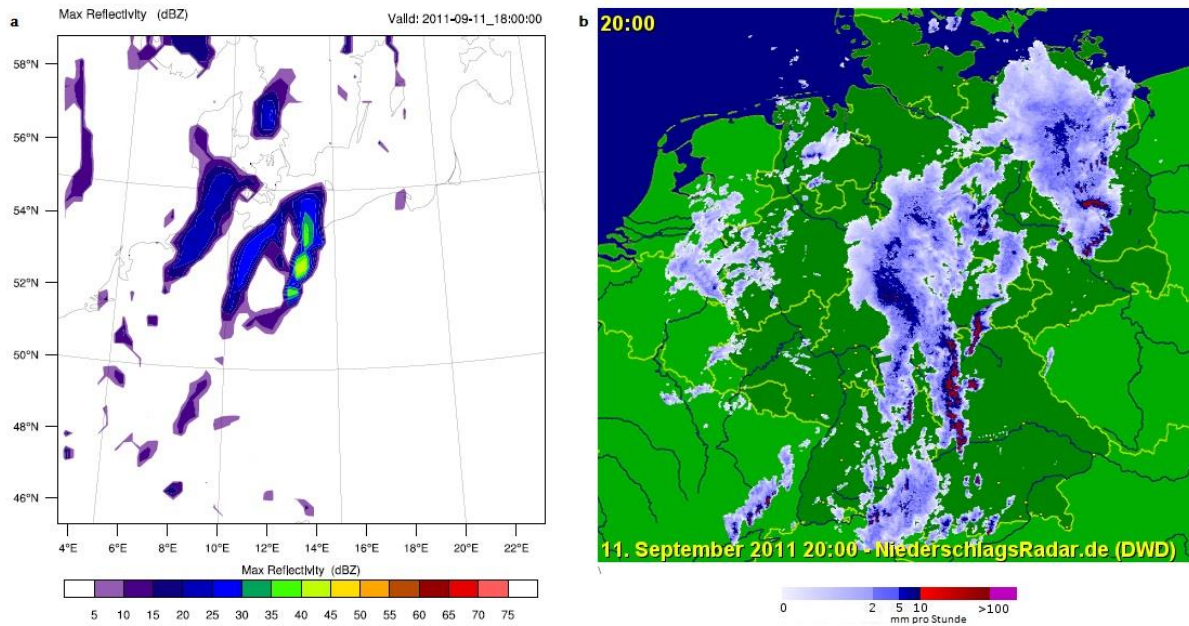| Numerical and physics process	WSM6_NOAH_MYJ_KF
Microphysics	WSM6 scheme
Longwave Radiation	RRTM scheme
Shortwave Radiation	Dudhia scheme
Surface Layer	Janjic scheme
Land Surface	Noah Land Surface Model
Planetary Boundary Layer	Mellor–Yamada–Janjic scheme
Cumulus Parameterization	Kain–Fritsch scheme
Start time	September 11, 2011 12.00 UTC
End time	September 12, 2011 18.00 UTC

3.1.4 Validation of the reference run

The start time of figure 5 is September 11, 2011 at 15.00 UTC and ends on September 12, 2011 at 00.00 UTC. The first squall line is around 19.00 UTC, the second line of light showers passed over Berlin around 22.30 UTC.

Figure 5. *The modelled (dashed line) and observed (solid line) precipitation of the four Wunderground weather stations in the urban area of Berlin is plotted against the time [UTC]. The modelled and observed precipitation [mm] peak was between 18.00 and 21.00 UTC in the city centre of Berlin.*
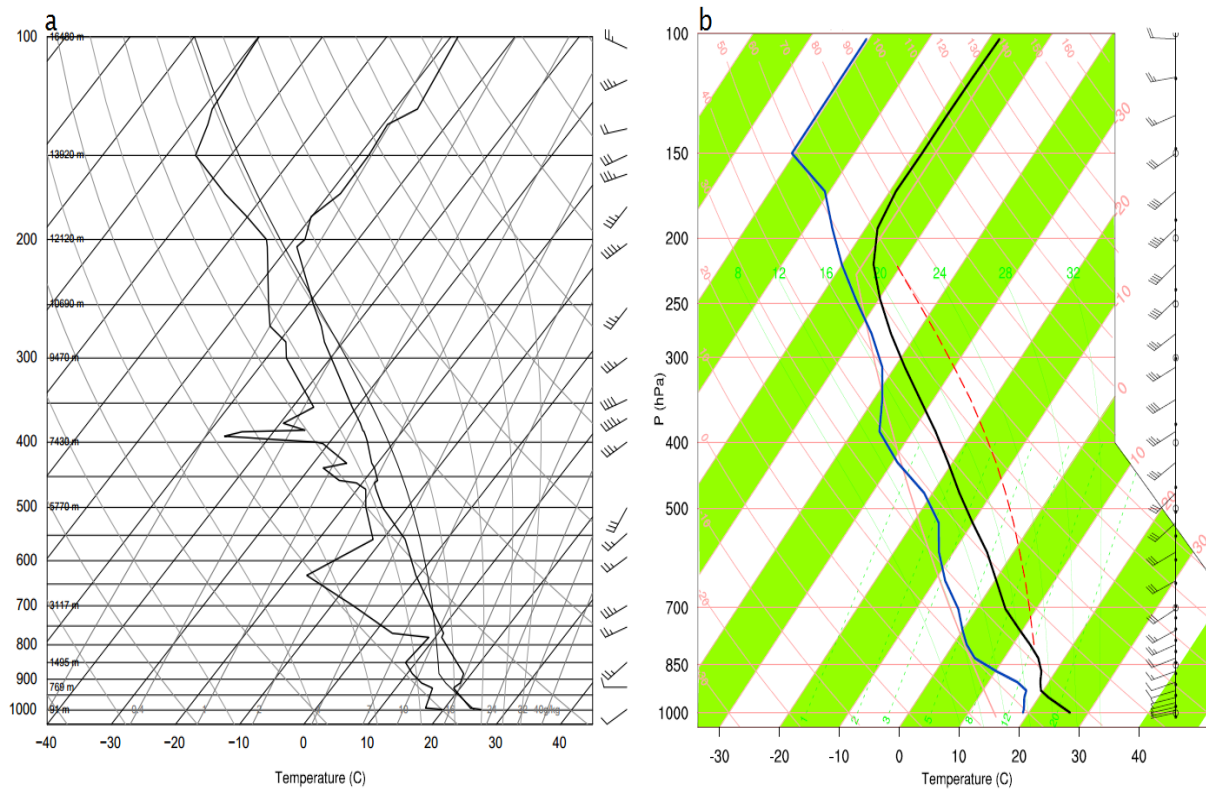
The modelled quantities of precipitation were on average higher than the Wunderground weather station observations on four locations in Berlin. However, some extremes are simulated for stations IBERLINB15 and IBERLINB24 at 19.00 UTC. The precipitation of the WRF model simulated 13 to 16 [mm] higher values than the observations for the two locations (figure 5). The difference was caused by a more intensive modelled squall line over the southern part of the city than in the observations. This was possible due to higher maximum temperatures along with a too early development of the first squall line. The timing of the second squall line was more accurate to the actual situation (figure 6). The first squall line is shown in figure 6a and is located between the latitudes 12°E–14°E and has three areas of higher precipitation intensities (peak at 45 [dBZ]). The location of the first squall line is visible on the radar in the eastern part of Germany, with a maximum reflectivity of 45 [dBZ] (figure 6b). In the following hours, the shower activity of the first squall line decreased.

Figure 6. _The radar reflectivity over Germany at 18.00 UTC (20.00 LT) in a) the WRF model and b) the radar observation (source: www.niederschlagsradar.de)._

The second squall line is simulated at 10°E with a maximum reflectivity of 30 [dBZ]. The modelled second squall line developed during the hours after that, but the maximum reflectivity went north of Berlin. The observed second squall line is located in the central and southern part of Germany in figure 6b. The modelled third squall line, located at south Denmark at 18.00 UTC, extinguished in the following hours.

Last part of the reference run was the comparison between the observed sounding of the Lindenberg (rural area) and the two modelled soundings of the WRF model (urban and rural area) (figure 7). The urban surface temperature in the sounding of the WRF model was max. 0.87 [°C] higher than the sounding of the WRF model in the rural area (not shown). The surface temperature difference in the observed sounding of Lindenberg was about 0.50 [°C] lower than in the modelled sounding in the rural area. The dewpoint temperature was in both figures approximately 20 [°C]. In the WRF model, the difference between the temperature and the dewpoint temperature decreased as the height increased in the lower part of the atmosphere. Between 500 and 800 [hPa], the WRF model simulated a layer with a lower moisture content. The moisture content in this layer was lower in the urban area than in the rural area of the modelled sounding (not shown). The tropopause is located at 200 [hPa]. In the observed sounding, the tropopause began at 200 [hPa] and there was a dry layer between 500 and 800 [hPa] as well. However, in Lindenberg's sounding there was an extra relatively thin layer with lower moisture content at a height of 400 [hPa].

Figure 7. The soundings of September 11, 2011 12.00 UTC, a) observed in Lindenberg (rural area near Berlin) and b) modelled sounding in the rural area near Berlin as well.
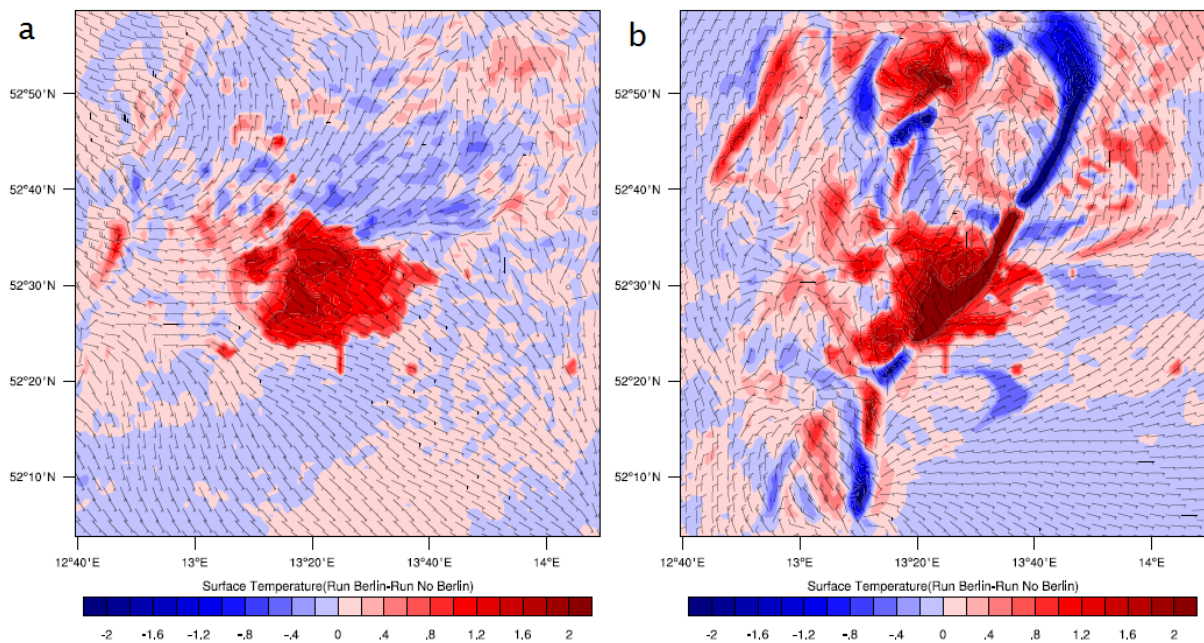
The CAPE was in Lindenberg's sounding $0.8 \cdot 10^3$ [J/kg] and $1.8 \cdot 10^3$ [J/kg] at 12.00 and 18.00 UTC respectively. In contrast, the CAPE values of the two modelled soundings were higher: in the rural area $2.4 \cdot 10^3$ [J/kg] and $2.0 \cdot 10^3$ [J/kg] and in centre of Berlin $2.1 \cdot 10^3$ [J/kg] and $1.8 \cdot 10^3$ [J/kg]. Thus, the higher precipitation in the WRF model (figure 5) indicated higher modelled CAPE values compared to the observed CAPE values.

3.2   Simulation of urban versus nonurban

This chapter discusses the impact of Berlin on the severe thunderstorm. The run with Berlin is compared with the run without Berlin in this case.

3.2.1 Temperature differences

The temperature differences between the model runs with and without Berlin have been investigated. The urban area is warmer than the rural area just before the first squall line passed over the city area. This temperature difference of the reference run was in the range of approximately 0.5–2.0 [℃]. Even the observations of Wunderground weather stations measured an urban heat island effect before the squall line passed the area of Berlin. In the urban areas, the observed temperatures were approximately 1 [℃] higher than in the rural area (not shown).
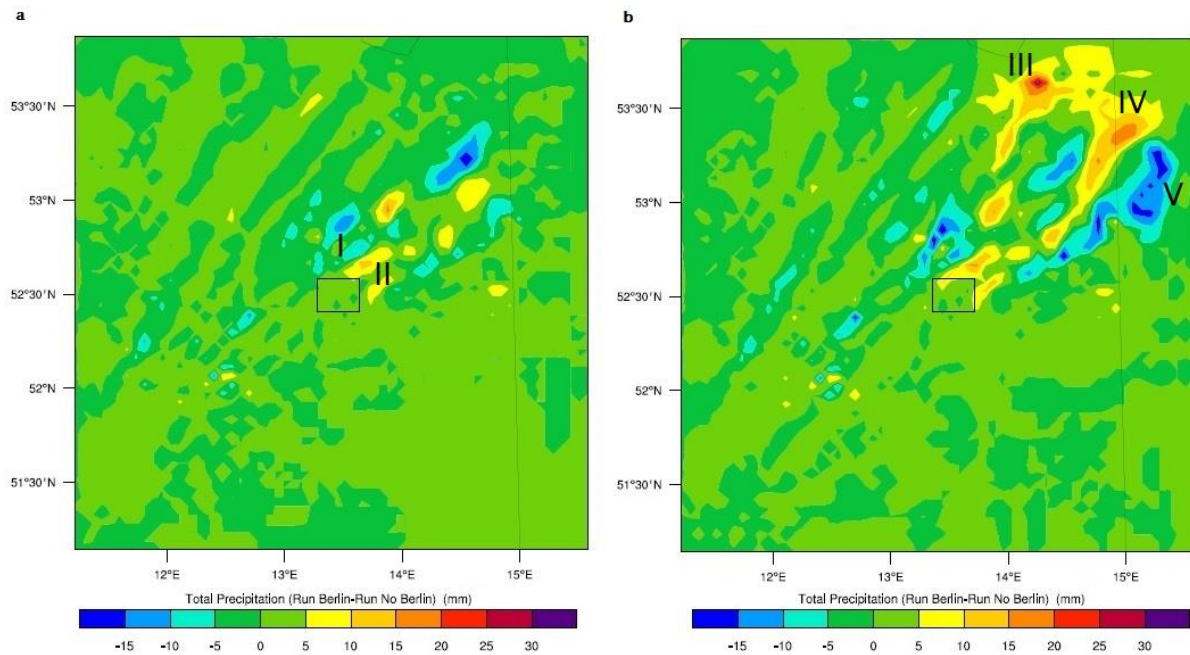

Figure 8. Temperature differences between the model run with Berlin minus the run without Berlin and the wind direction (arrows) at a) 16.50 UTC (before the first squall line) and b) 18.20 UTC (first squall line above urban area).

Figure 8b shows the modelled temperature of domain 3 at 18.20 UTC. The first squall line has been passed over the city centre. The temperature difference between the west side (warm air) and east side (cold air) of the first squall line was approximately 7 [℃] (not shown). The urban heat island effect decreased after the first squall line passed over Berlin. The convergence line had negative temperature differences to the north and south of Berlin (figure 8). One possible explanation has been the time difference of the squall line. The locations with higher negative temperature differences in the squall line suggest a higher intensity of precipitation and therefore more cooling of the surface temperature.

3.2.2 Precipitation differences

Next, the precipitation difference between the two WRF simulations has been investigated (figure 9). The differences are particularly visible in the downwind area of Berlin. The first squall line passed domain 2 from southwest to northeast. The surface wind direction has been northeast ahead of the squall line and west to northwest behind the squall line. In both figures there have been a scattered pattern of positive and negative precipitation differences, especially in the northwest area of the city Berlin.
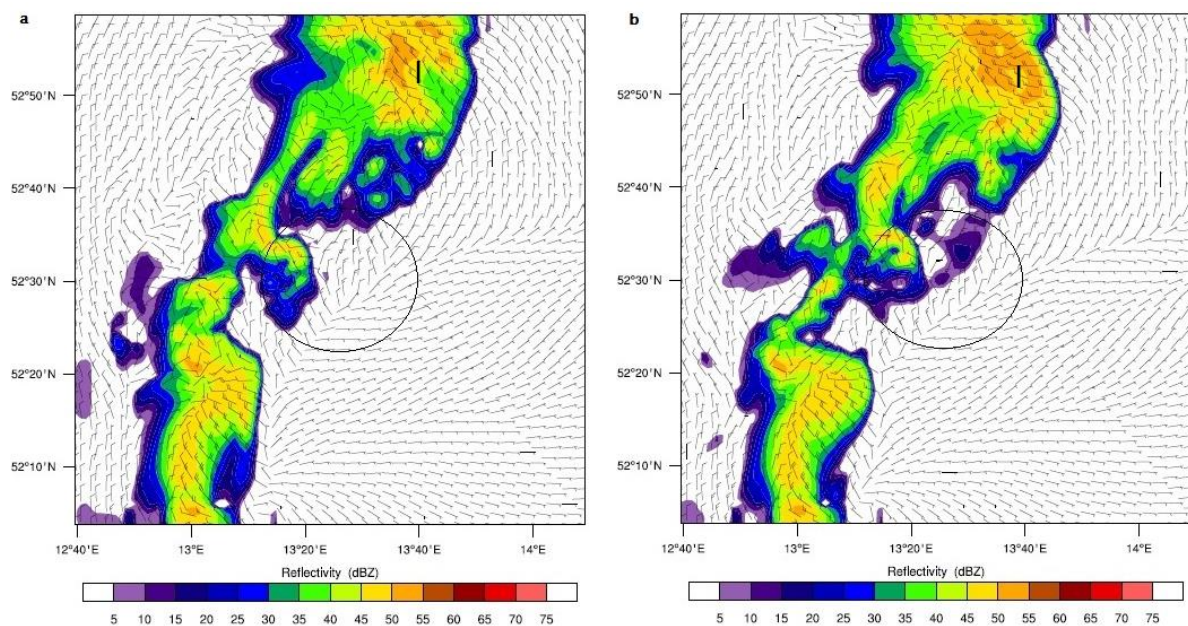

Figure 9. *The modelled accumulated precipitation differences in domain 2 with a) after the first squall line passed Berlin (21.00 UTC) and b) after the second line passed the city (24.00 UTC). The black square is the city Berlin.*

In the area north of Berlin (figure 9a, area I) the precipitation amount was higher in the model run without Berlin than in the model run with Berlin. In contrast, the area east of Berlin had a positive precipitation difference with a maximum of 15 [mm] (figure 9a, area II). In area III and IV (figure 9b) the precipitation differences were, after the second squall line has been passed, positive with a maximum difference of 25 [mm] in area III. Area V had a negative precipitation differences in an elongated area. There have been differences in precipitation in the urban area of Berlin as well. The largest part of the city had a small positive precipitation difference (less than 5 [mm]), but two areas in the city had a negative precipitation difference of less than 5 [mm]. On average, there was a small difference in the modelled accumulated precipitation in the urban area and area downwind of Berlin (selected area between 13°30'E–15°20'E and 52°30'N–53°45'N). The precipitation difference of the model run with Berlin was in the selected area approximately 2 percent lower compared to the model run without Berlin in the same area. The precipitation difference between the Berlin model run and the rural model run was small, but the frequency distribution suggest a small difference (figure 25). The urban histogram indicated a lower centre of gravity than the

rural histogram. The frequency of accumulated precipitation between 15 and 25 [mm] was higher in the model run with Berlin compared to the frequencies of precipitation without Berlin. The frequency of high accumulated precipitation (with more than 40 [mm]) was higher in the model run without Berlin than in the model run with Berlin (figure 25, Annex). This suggest a result of the presence of the city Berlin.

3.2.3 Possible causes for precipitation differences

The latent heat flux is an interesting variable because the flux is associated with evaporation of water at the surface and subsequent condensation of water vapour in the atmosphere. The positive latent heat fluxes have been consistent with the radar reflectivity. In the first squall line the latent heat flux was 50 [W/m^2] more positive than the surrounding area. However, due to the combination of low urban soil moisture content and a higher sensible heat flux above the urban area compared to the rural area, the latent heat flux dropped rapidly above the urban area (figure 23 and 24, Annex). As a consequence the line-shaped area with the positive latent heat bifurcated above Berlin. This area passed partly around the city and partly extinguished. However, the precipitation difference in the city area was slightly positive (figure 9).

Figure 10. *The radar reflectivity in domain 3 at 18.20 UTC for a) the model run with Berlin and b) the model run without Berlin. The black circle is in (a) the city Berlin and (b) an indication of the urban area of Berlin.*

In the run without the urban area of Berlin, the latent heat and upward moisture flux did not split up due to a higher soil moisture in the rural area. This kept retained the line-shape area. The radar reflectivity didn't show an interruption of the latent flux (figure 23, Annex). It appears that the modelled accumulated precipitation, averaged over 9 locations in the urban area, was 3.6 percent less compared to the same locations in the model run without Berlin. This was caused by a combination of a high sensible heat flux and low latent and moisture

fluxes over the area of Berlin (mechanism II). Area I with reflectivity higher than 50 [dBZ] north of Berlin has been increased in the model run without Berlin compared to the run with Berlin (figure 10). After the first squall line passed Berlin, the line structure of the latent heat flux restored and enhanced even downside of Berlin compared to the model run without Berlin, resulting in a positive precipitation difference in some parts in the downwind area of Berlin. Overall, there has been a small difference in modelled accumulated precipitation downwind of the city.
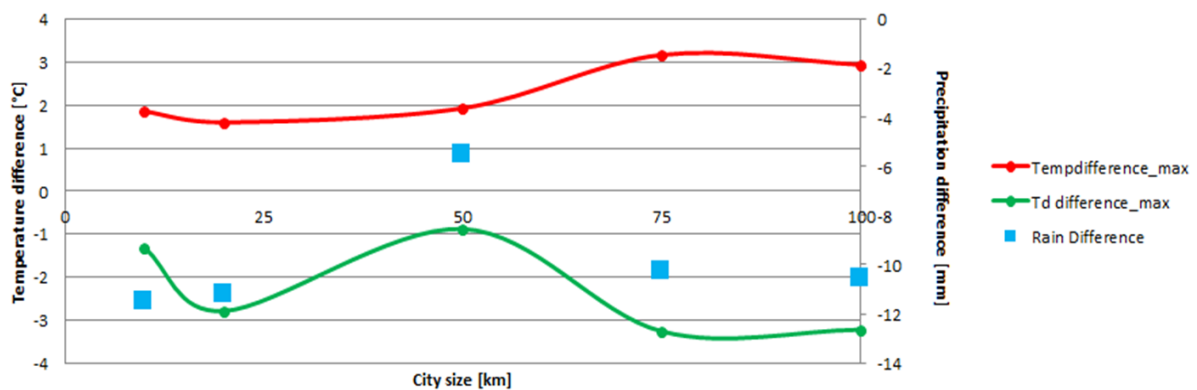
3.2.4 Instability

The instability (CAPE) was in the urban area $0.2 \cdot 10^3$ [J/kg] lower than in the run without Berlin (not shown). Although the temperature was 0.5 to 2 [℃] higher in the urban area than in the rural area, the moisture effect influenced the CAPE values in the urban and rural areas. This result indicated that the instability has been decreased in urban areas due to the dominance of the lower dewpoint effect. In combination with the decreased latent heat flux and increased sensible heat flux, this corresponded to mechanism II.

3.3 Influence city size on convective precipitation

This section shows the results of the influence of the city size on precipitation. For five different city diameters, the effect on the (dewpoint) temperature and precipitation patterns in and around a particular city diameter has been investigated.

3.3.1 Effect city size on temperature and precipitation

Figure 11 shows the city size against the modelled maximum (dewpoint) temperature and precipitation in the centre of the selected cities. Cities with a diameter of 10, 20, 50, 75 and 100 kilometres have been investigated. Before the first squall line passed an urban area, the local urban heat island effect has been investigated. Figure 11 shows that with increasing city size the urban heat island linear increased as well, approximately 0.33 [℃] per 20 kilometres city diameter. The city of 20 kilometres had an urban heat island effect of 1.5 [℃]. According to Schmid (2013), the average maximum heat island over the urban area for similar city size is approximately 1.0 [℃]. Our results suggest that the urban heat island effect did not continue to increase for city sizes larger than approximately 75 kilometres. This result is in contrast with the result of Schmid (2013). According to Schmid (2013), the urban heat island became constant for cities larger than 20 kilometres. However, the levelling off is consistent.
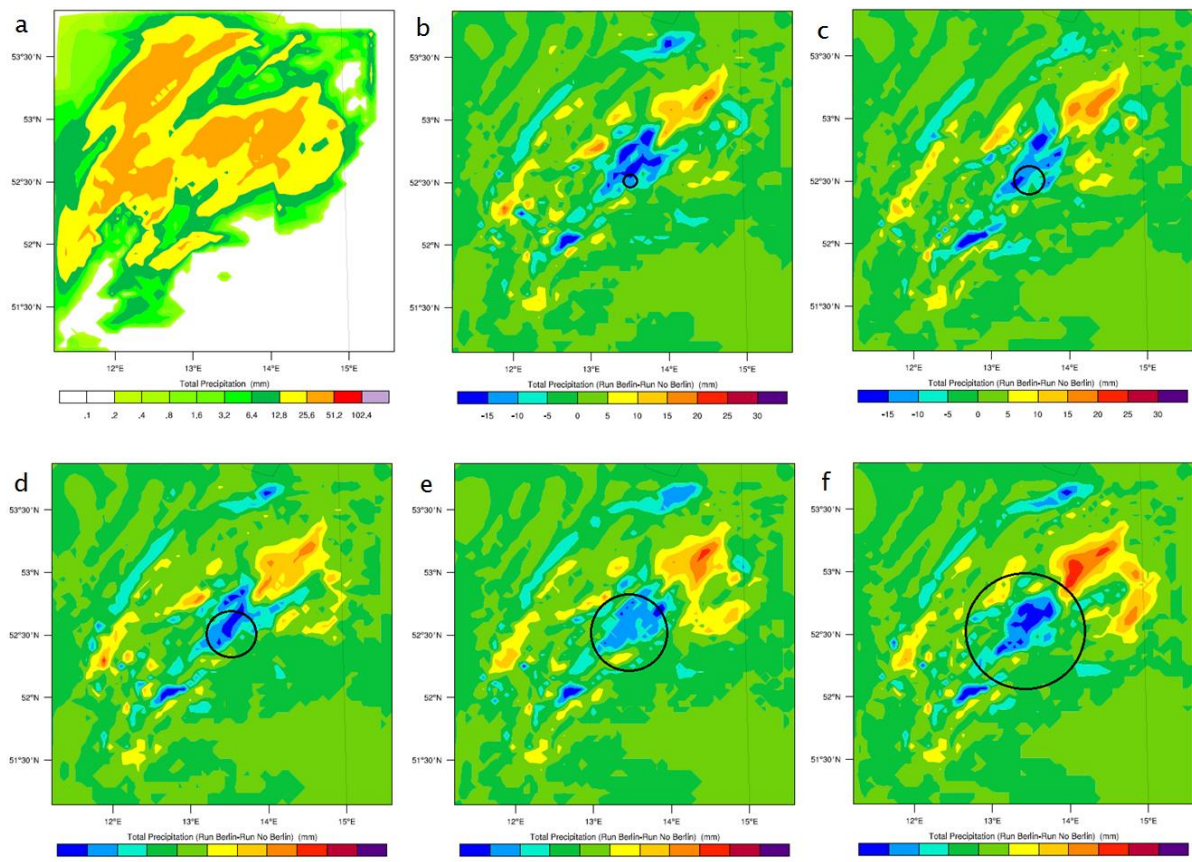

Figure 11. *The temperature (red line) and dewpoint (green line) temperature differences between urban and rural area has been plotted against the five city sizes.*

The dewpoint temperature has been studied for the different city sizes as well. Figure 11 show that the urban heat island effect affects the dewpoint temperature difference between the centre of a city and the rural area. With an increased city size, the dewpoint temperature decreased due to less precipitation. According to Schmid (2013), the dewpoint temperature decreased linearly with increasing city size, due to the moisture air of the surrounding rural area. Remarkable is the small dewpoint temperature difference for the city with a diameter of 50 kilometres. This is probably caused by the one point measurement in this case instead of an average dewpoint temperature over multiple grid cells in the urban area.

3.3.2 Precipitation in urban areas

The differences in modelled accumulated precipitation between the model runs with the urban area and without urban area at 21.00 UTC show scattered patterns in the downwind and leeward area of the urban area. The model run with the original Berlin (Case 2) only showed accumulated precipitation differences on the downwind area and not on the leeward area of the city at 21.00 UTC.

The first squall line passed the domain from southwest to northeast. Most accumulated precipitation was simulated in the central and north-western part of the domain. The black circles in figures 12b to 12f were the indications of the selected city sizes.

Figure 12. *The precipitation differences between the urban model run and the model run without the city. The urban area has been indicated by a black circle. The figures with different city sizes showed differences in precipitation in the whole domain and in the urban area itself.*

In figure 12b to 12f the precipitation differences are plotted between the run with the circular city and the run without urban area. Remarkable was the precipitation difference in the urban areas. The WRF model has been simulated less accumulated precipitation in the centre of the urban areas, but more precipitation in the suburbs of cities larger than 50 kilometres. There was, averaged over 4 urban grid cells in the 10 kilometres city to 54 urban grids cells in the 100 kilometres city, approximately 15 percent less accumulated precipitation in the five urban areas than in the model run without urban area. Five
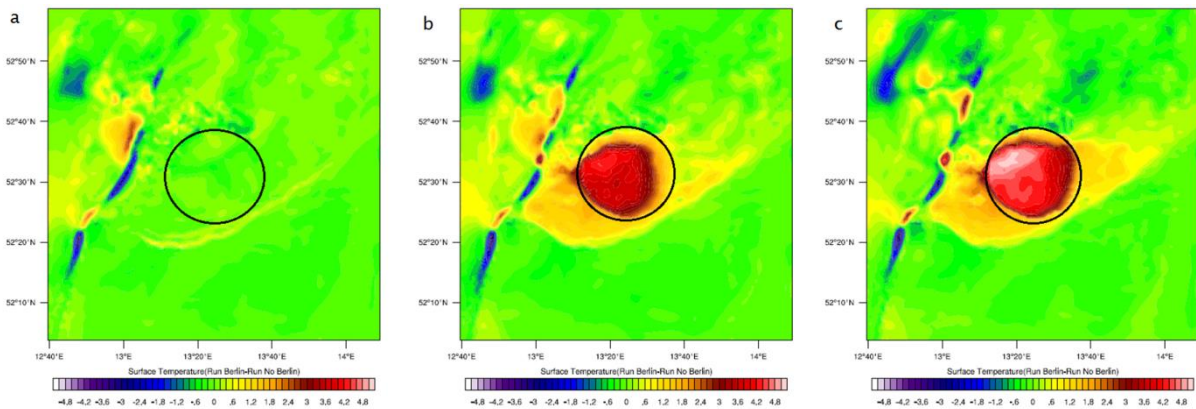
histograms (selected area between 13°30'E–15°20'E and 52°30'N–53°45'N) indicated an increase in the precipitation frequency as the city size increased, in case of a precipitation amounts between 5 to 15 [mm] and more than 25 [mm]. The precipitation frequency between 15 and 25 [mm] was higher for smaller city sizes.

3.4　Impact of anthropogenic heat on urban precipitation

The emission of anthropogenic heat (H_A) causes an increased urban heat island effect (Bohnenstengel et al., 2013). The anthropogenic heat shows a daily cycle for London (Bohnenstengel et al., 2013). This case investigates the influence of four values of anthropogenic heat in the urban area on the first squall line. The anthropogenic heat in the urban area had maximum values of 2, 40 and 100 [W/m²] and have been compared with the urban run without anthropogenic heat.

3.4.1 Temperature difference with versus without anthropogenic heat

The anthropogenic heat created an additional warming in and around the urban area compared to the urban area without anthropogenic heat (Case 3, city size of 20 [km]). This is plotted in figure 13 at 17.30 UTC, the time just before the first squall line passed the urban area. In the centre of the urban area, the temperature difference of the city with a maximum of 100 [W/m²] anthropogenic heat was the largest (approximately 4 [℃]) compared to the urban area without anthropogenic heat. According to Taha (1997), an anthropogenic heat between 20 and 40 [W/m²] can create an urban heat island of approximately 2–3 [℃] warmer compared to the surrounding area. The temperature of an urban area with a maximum of 40 [W/m²] anthropogenic heat indicated an urban heat island of 3 [℃] warmer than the rural area. Differences in the urban vegetation fraction and dark urban surfaces can enhance the urban heat island.
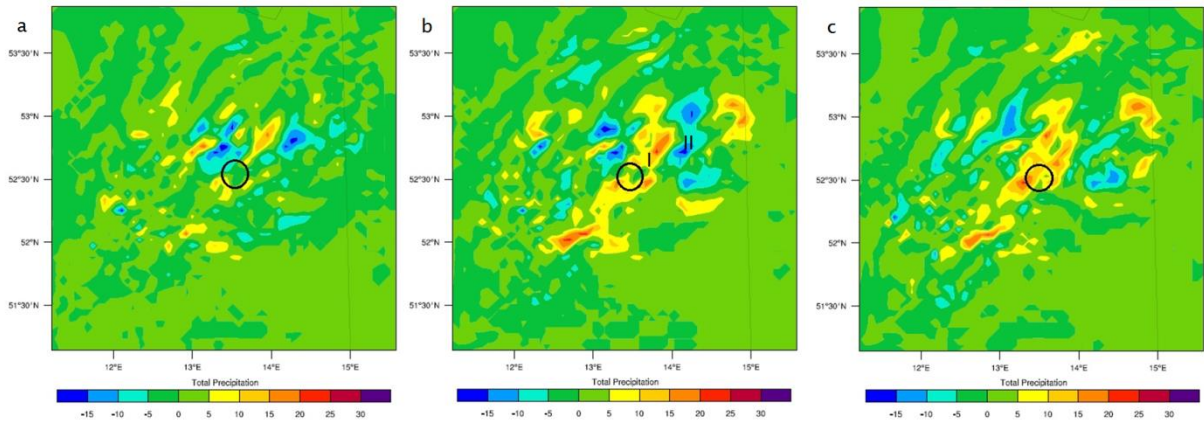

Figure 13 *The temperature differences in a) between the lowest anthropogenic heat in the urban area and the urban area without anthropogenic heat, b) between 40 [W/m²] anthropogenic heat in the urban area and the urban area with no anthropogenic heat and c) between the model run with the highest anthropogenic heat in the urban area and the model run without anthropogenic heat.*

Due to the induced southeast wind by the convergence to the squall line, the area with positive temperature differences in the urban area expanded to the western area of the urban area (figure 13b and 13c). The urban area heated up rapidly after the passage of the convergence line over the urban area, especially the urban area with a maximum of 100 [W/m²]. The increase of the urban temperature was approximately 1.6 [℃] in 40 minutes.

3.4.2 Impact on precipitation in and around city area

The precipitation differences of the urban areas with anthropogenic heat are plotted against the urban areas without anthropogenic heat in figure 14. In the model runs with a maximum of 2 [W/m²] anthropogenic heat, the WRF model simulated slightly less rainfall in the city centre than in the urban area without anthropogenic heat. However, WRF simulated more precipitation in the urban area with an anthropogenic heat of 40 and 100 [W/m²]. This was caused by the impact of anthropogenic heat in the urban areas on precipitation. The CAPE values were on averaged $0.80 \cdot 10^3$ [J/kg] higher in the urban areas with anthropogenic heat of 40 and 100 [W/m²] compared to the urban area without anthropogenic heat (not shown). The combination of higher CAPE (destabilized effect), sensible and latent heat fluxes in the urban area resulted in more precipitation in the urban area with 40 and 100 [W/m²] than in the urban area without anthropogenic heat. This result corresponded to mechanism I.

Figure 14. *The modelled precipitation differences at 21.00 UTC between a) the model run with a maximum of 2 [W/m²] anthropogenic heat minus the urban area without anthropogenic heat, b) the model run with 40 [W/m²] anthropogenic heat in the urban area minus the urban area without anthropogenic heat and c) the model run with the highest anthropogenic heat minus the urban area without anthropogenic heat.*
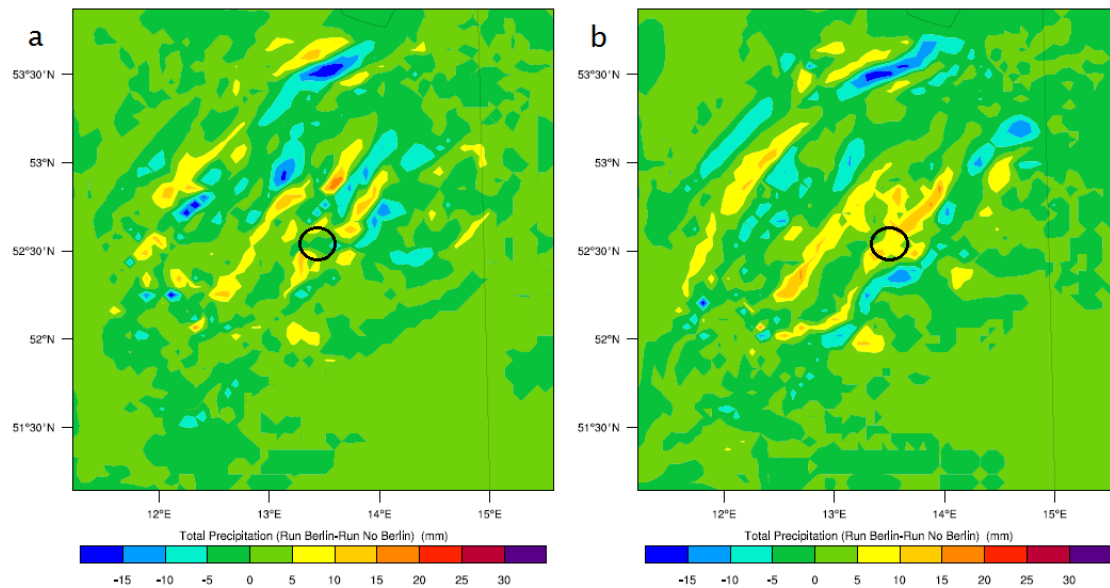
In the urban area with an anthropogenic heat of 40 [W/m²], the CAPE amounted $1.9 \cdot 10^3$ [J/kg]. In the urban downwind area, the CAPE value was $1.3 \cdot 10^3$ [J/kg] (figure 14b, area I). The CAPE value was $1.1 \cdot 10^3$ [J/kg] in area II (figure 14b). This result suggest that the precipitation increased in the urban area and in area I, due to an increased instability and anthropogenic heat. However, the precipitation decreased in area II, which indicate advection of stabilized air from area I to area II. In other words, warm air is advected over colder surface in area II (figure 14b) and results in less precipitation compared to area I (figure 14b).

3.5   Building height in the urban area

The city size was not expanded in this section, but the buildings in the urban area became smaller and larger. In the WRF model, the building heights have been linked to the roughness lengths and displacement heights. Three model runs have been investigated with different building heights, namely 1.5, 7.5 and 15.0 metres height.

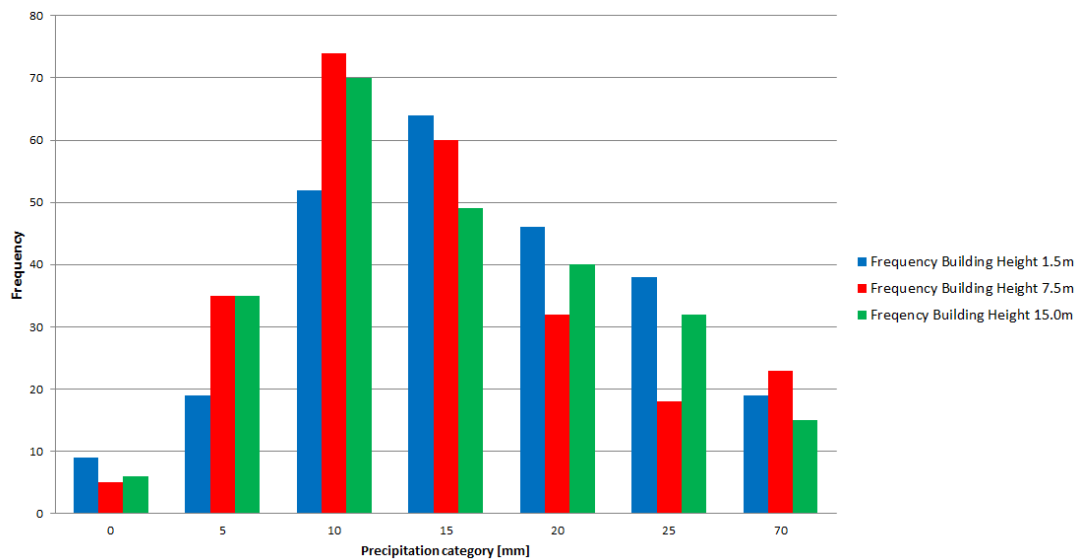### 3.5.1 Precipitation differences

Figure 15 illustrates the modelled precipitation differences between the urban area with the building heights of 7.5 and 15.0 metres and the precipitation in the 1.5 metres height urban buildings. Through this approach we can capture one specific city feature effect on the convective precipitation and exclude the urban effect. Figure 15 shows that with increasing building height, the precipitation increases in the urban area, in the leeward and in the downwind areas compared to the model run with the lowest building height. The latent heat flux increases in the leeward area of the urban area as the urban building height increases, which resulted in a positive precipitation difference. The average accumulated precipitation was approximately 14.7 percent higher in and downwind of the urban area with the highest buildings (selected area between 13°30'E–15°20'E and 52°30'N–53°45'N), compared to the same area of the model run with the lowest building heights.

Figure 15. *The differences in precipitation between the urban area differences between a) the building height of 7.5 metres minus the building height of 1.5 metres and b) the building height of 15.0 metres minus the building height of 1.5 metres in the second domain.*

The precipitation distribution with the lowest urban building height shows the highest frequencies between 15 and 25 [mm] precipitation in the urban and downwind area, compared to the histograms of the higher buildings in the urban area. Precipitation less than 15 [mm] and more than 25 [mm] have lower frequencies compared to the frequencies of the model runs with higher building heights. The centre of gravity of the histogram with the

28

lowest building height is between 15 and 20 [mm], while the centre of gravity for the higher building height histograms is between 10 to 15 [mm].
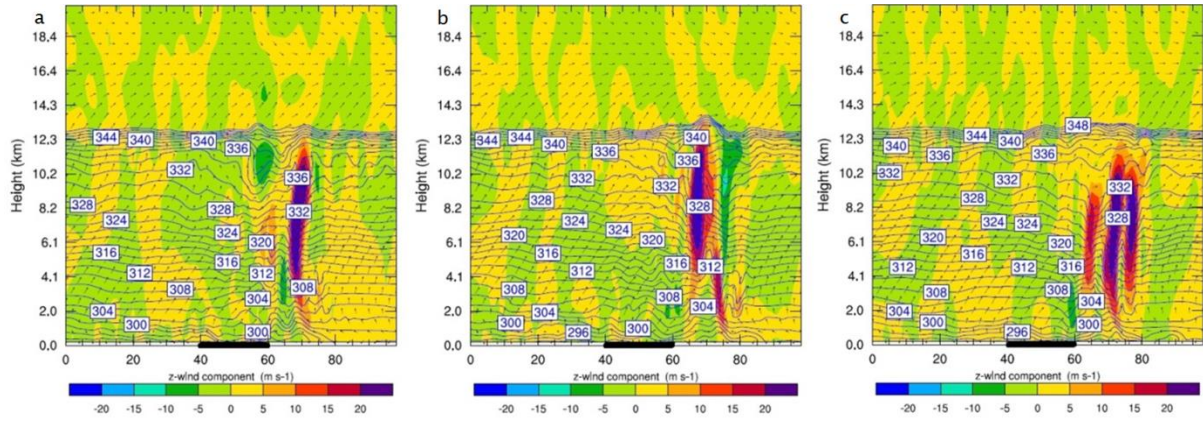
3.5.2 Instability

The CAPE value in case of the highest urban building height was lower than in the model runs with lower building heights (not shown). In the centre of the urban area, the CAPE value was between $2.3 \cdot 10^3$ and $2.5 \cdot 10^3$ [J/kg]. The instability in the urban area was on average lower than in the rural area (southwest part of domain 3), due to a lower moisture content and temperature in the urban area.

Extra heat is advected into the urban area by an area of divergence located on the north side of the urban area before the first squall line passed the urban area. However, warm urban air is advected to the rural area due to an area of convergence on the south side of the urban area. The turbulence in the urban area increases due to the increase of the urban roughness. As a consequence, the heat at the urban surface is mixed with dry and cooler air through the turbulence (entrainment effect) and as a result, the instability and temperature decrease in the urban area.

3.5.3 Cross sections city area

The west-east cross section is plotted in figure 17, whereby the urban area is marked with a black bar under the x-axis. Time of the cross section is 19.10 UTC, when the first squall line just passed the urban area. In figure 17a the situation with 1.5 metres buildings in the urban area is plotted.

Figure 17. *The west–east cross sections in the third domain at 19.10 UTC. The convection, wind direction and the potential temperatures are plotted. In a) the cross section of the urban area with a building height of 1.5 metres is shown, in b) the model run with a building height of 7.5 metres and in c) the urban area with a building height of 15.0 metres is plotted.*

The convection is located east of the urban area (figure 17). Figure 17 also shows the area of subsidence is located on the edge of the rural and urban area due to the extra roughness and therefore divergence. The convective areas indicated areas with increased precipitation. In the area east of the cities with building heights of 7.5 and 15.0 metres have higher precipitation values than the city with a building height of 1.5 metres (figure 15b). This result suggests that a stronger convection caused more precipitation.

In the urban area with a building height of 7.5 metres, the convection reached a higher level in the atmosphere compared to the urban area with the smallest buildings. On both sides of the convection there were areas of subsidence. In figure 17c the cross section is plotted for the urban area with the largest buildings. There were three convection areas east of the urban area. In addition, the part of the atmosphere above the urban area had a positive vertical velocity. In figure 17a and 17b was the opposite situation. The building heights (linked to the roughness lengths and the displacement heights) suggest destabilisation of the air and convection from the suburban area to 25 kilometres downwind of the urban area (correspond to mechanism I). Same situation has been valid for the southwest–northeast cross section (not shown). The size of the convection area in the downwind areas was difference. The area of convection has been reduced by half and the strength of the vertical wind speed has been slightly reduced compared to the convection areas in the west–east cross section.
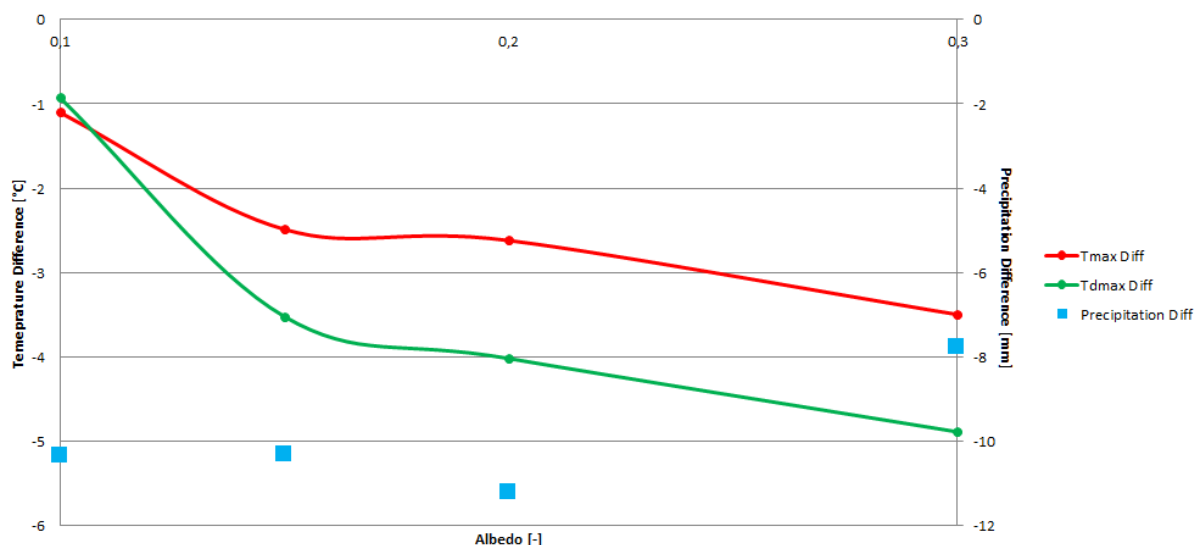
The convergence in the model runs with an urban area was stronger than in the model run without city. With increasing building height, the area of convergence increased in and around the urban area. The convergence line is delayed in the model run with the highest buildings compared to the run with no and small buildings. This suggest that there was a blocking effect of buildings in the urban area as the building height increased.

3.6 Various albedos in city centre

Most European and American cities have an urban albedo between 0.10 and 0.20 [–]. In the centre of an urban area, the albedo is close to 0.10 [–] and in the suburbs close to 0.20 [–]. This difference is partly caused by the vegetation in an urban area and the ratio sensible heat flux and vertical wind speed. The difference in albedo in an urban area had impacts for the temperature, precipitation and net shortwave radiation in and around the urban areas.

3.6.1 Effect albedo on (dewpoint) temperature

Figure 18 shows the temperature and the dewpoint temperature differences between the urban and the rural area. When the albedo increases in the urban area, the net solar radiation decreases due to the factor $(1-\alpha)$ from equation [1] (Chapter 1.1). As a consequence, the temperature decreases in the urban area (figure 18). In this case, the average temperature decrease was approximately 0.7 [°C] per 0.10 albedo. The dewpoint temperature decreases in the urban area as the albedo increases, as a result of the decreasing temperature and relative humidity.

Figure 18. The temperature (red line) and dewpoint (green line) temperature plotted against the albedo in the centre of the urban area. For an albedo of 0.3, the WRF model simulated 2 millimetres more precipitation in the centre of the urban area compared to the model runs with a lower albedo.
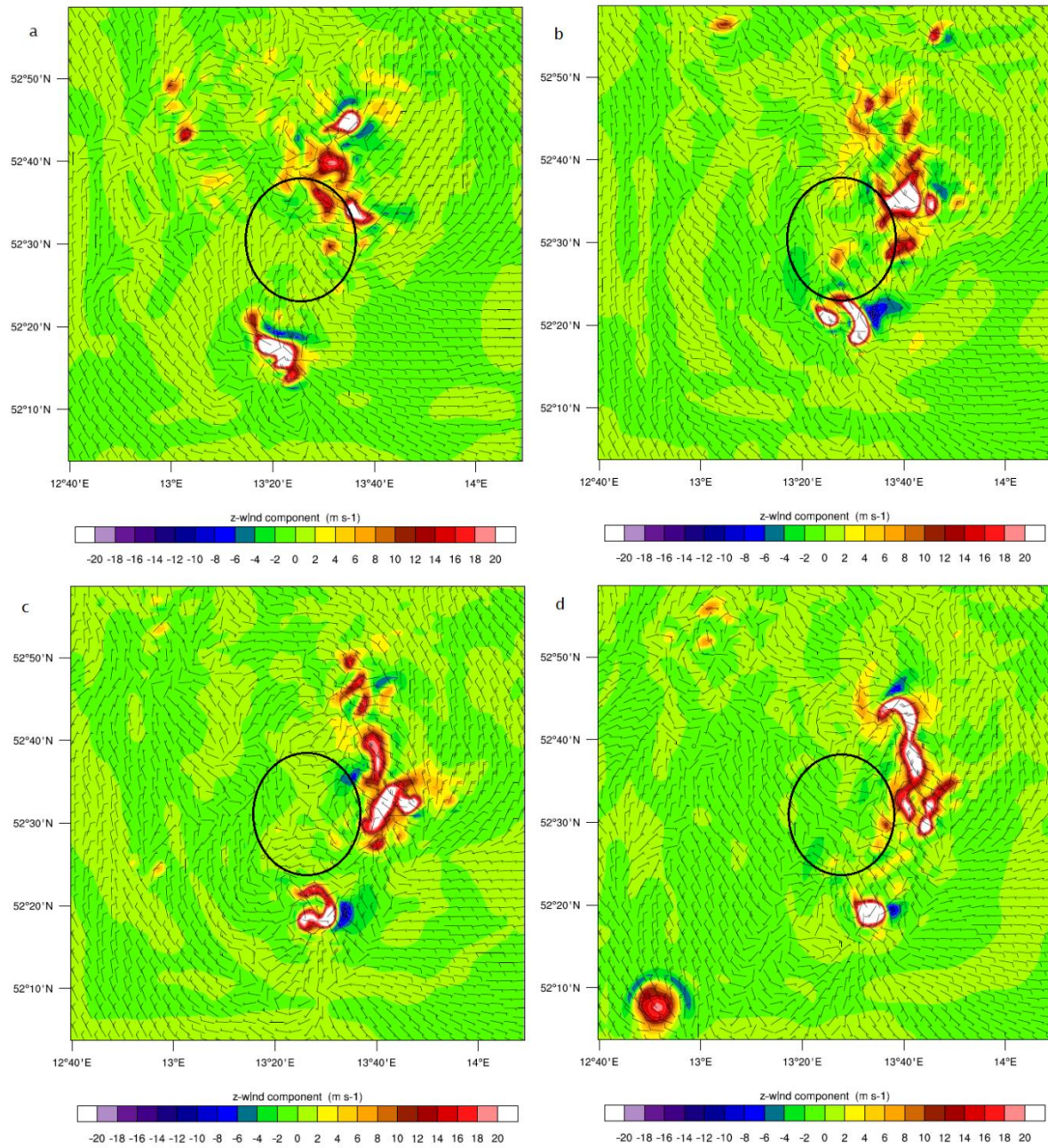
3.6.2 Impact albedo on the precipitation, instability and convection

The accumulated precipitation in the urban areas was on average approximately 3.8 percent higher than in the rural run (9 precipitation measurements per urban albedo). The precipitation decreased in the urban area with an albedo between 0.10 and 0.20 [–]. A higher urban albedo resulted in a lower net shortwave radiation and a lower temperature, which resulted in a lower sensible heat flux, a lower latent heat flux and less precipitation in the urban area (figure 27, Annex).

The precipitation in the urban area decreases as the urban albedo increases. The CAPE value in the urban area with the highest albedo was lower than in the model runs with lower urban albedo (not shown). In the urban area with an albedo of 0.1 [−], the CAPE value was approximately $0.25 \cdot 10^3$ [J/kg] higher than in the urban area with the highest albedo value. However, the precipitation increased in case of an urban albedo of 0.30 [−]. This suggests the higher surface temperature and sensible heat flux cause a thicker boundary layer with entrainment of dry air. As a consequence, the precipitation decreases in case of an urban albedo equal or smaller than 0.20 [−]. In case of an urban albedo of 0.30, the increase of urban precipitation suggests that the instability and temperature has been decreased due to the dewpoint effect.

The vertical wind speed is plotted in figure 19. The figure shows the areas with positive vertical velocity passed over the urban area which resulted in strong convection areas south and northeast of the urban area.

The vertical velocity averaged over the urban and downwind area (selected area between 13°25'E–14°05'E and 52°30'N–52°55'N) was 0.01 [m/s] in the model run with an urban albedo of 0.10 [−]. In the model runs with an urban albedo of 0.15 and 0.20 [−], the vertical velocities were 0.58 [m/s] and 1.36 [m/s] respectively. The vertical velocity was on average −0.40 [m/s] in the model run with the highest urban albedo. These results suggest that as the urban albedo is equal or smaller than 0.20 [−], the vertical velocity is positive (convection) and indicate a small increase of precipitation in the selected area, which correspond to mechanism I.
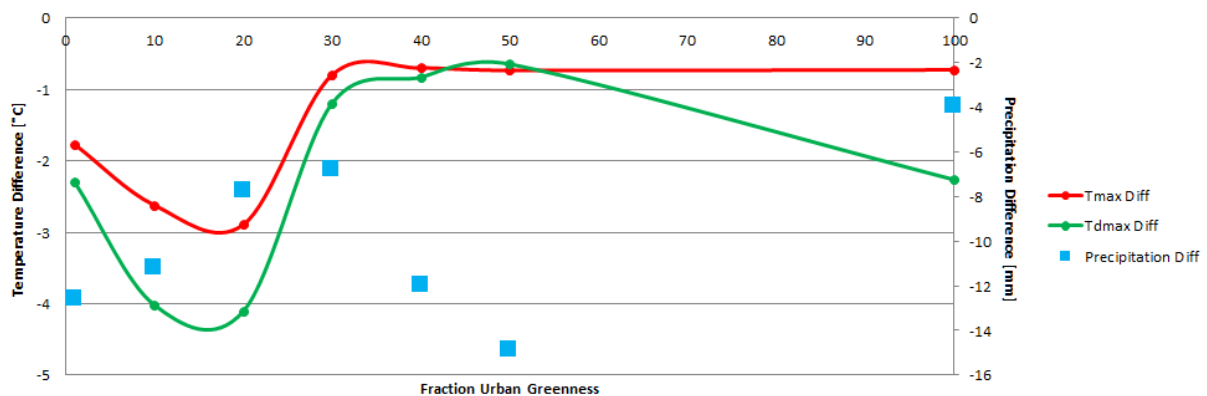
Figure 19. The areas with convection (positive vertical wind speed) and subsidence (negative vertical wind speed) in and around the urban area of Berlin on September 11, 2011 19.10 UTC. The model run with a) an albedo of 0.1 [–], b) albedo of 0.15 [–], c) an albedo of 0.20 [–] and d) an albedo of 0.30 [–] in domain 3.

3.7   Vegetation cover in urban area

The effect of a vegetation cover in the urban area on a severe thunderstorm has been investigated in this section of the thesis. In this study, seven different vegetation covers have been selected for the WRF simulations. The vegetation cover were 1, 10, 20, 30, 40, 50 and 100 percent in the urban area.

3.7.1 Impact vegetation cover on (dewpoint) temperature

Figure 20 shows the minimum (dewpoint) temperature differences between the urban area with difference green fractions and the model run without city. As the vegetation cover in the urban area increased, the temperature difference indicated a decrease between the urban run and the rural run. The urban area indicated a cooling effect of approximately 0.06 [℃] for each 10 percent vegetation cover increase in the urban area. According to Theeuwes et al. (2012), the vegetation reduces the urban temperature, typically 0.6 [℃] for each 10 percent vegetation cover increase. The difference between the two simulations was approximately a factor 10, which was caused by experimental set-up differs. In case of Theeuwes et al. (2012), the research used a 1D model and this study used a 3D simulation.

Figure 20. *The temperature (red line) and dewpoint (green line) temperature plotted against the vegetation covers in the centre of the urban area.*

The dewpoint temperature indicated a slight decrease as well, namely 0.07 [℃] for each 10 percent vegetation cover increase in the urban area. In the situation of an increased urban vegetation cover, the difference between the urban dewpoint temperature and rural dewpoint temperature became smaller, which indicates more humid air. This was most likely due to the increase of precipitation and less heat in the urban area as the urban vegetation cover increases. The smallest (dewpoint) temperature difference between the urban and rural model was 0.6 [℃] in case of an urban vegetation fraction between 30 and 50 percent. The temperature difference of 0.6 [℃] did not decreases as the vegetation cover continue to increase. This can be caused by the land use category differences: the urban vegetation cover had cropland and grassland mosaic (LU=5), and the rural area had dryland, cropland and pasture (LU=2).

3.7.2 Impact green fraction on precipitation

The amount of precipitation in and downwind of the urban area increased as the green fraction in the urban area increased as well. This was the result of the smoothening of the urban area with an increasing green fraction in the urban area, which caused an increased wind speed (not shown). Another effect was the increase of the latent heat flux and the decrease of the sensible heat flux in the centre of the urban area due to the increased urban vegetation cover (correspond to mechanism II). The water vapour arose from the evapotranspiration of the vegetation. However, for urban areas with a green fraction of 30, 40 and 50 percent the latent heat flux was not larger than 50 [W/m^2] less than in the urban areas with a green fraction of 1, 10, 20 and 100 percent (figure 26, Annex). The lower values of the three latent heat fluxes was probably caused by the UCM variable 'BETR' (moisture availability of roof). In case of a rain rate of 1.0 [m/h] and higher, the BETR value changed from 0.0 [–] to 0.7 [–].

The increasing green fraction in the urban area caused a smoother urban surface and stabilization of the urban boundary layer. The velocity of the first squall line is affected by the smoother urban surface as well (not shown). In the model run with a green fraction of 1 percent, the squall line noticeably slowed down through the higher roughness of the urban area. The radar reflectivity intensified in the model runs with high green fractions, resulting in higher precipitation in and the downwind area of the urban area (figure 28, Annex). In the downwind area of the urban area the precipitation decreased as the green fraction increased.

4   Discussion

Previous studies have shown diverse results on the impact of an urban area on convective precipitation. On the one hand, there are studies that show an increase in urban precipitation (e.g. Changnon et al., 1990; Guo & Wang, 2006) and on the other hand there are studies that show a decrease in urban precipitation (e.g. Wan & Zhong, 2013). The study of Changnon et al. (1990) suggested an increase of urban precipitation of 13 to 15 percent (based on observations). According to the research of METROMEX, the precipitation increased by 5 to 25 percent in the downwind area of the city (Changnon et al., 1981; Wan & Zhong, 2013). The study executed in this master thesis investigated the impact of urban features on convective precipitation. The results show differences of approximately -2 to +14.7 percent precipitation in and downwind of the urban area. These results are comparable to the results of Changnon et al. (1990) and METROMEX. A deeper exploration of the two mechanisms has not been included in this study.

This study investigated the situation of a squall line in Berlin on September 11, 2011. In this situation, the squall line was located in front of a cold front. In addition, there are isolated summer thunderstorms as well, which occurs over very warm surfaces on a warm summer day. Since the isolated thunderstorms occur on a local scale, it would be a great challenge to simulate an isolated over the urban area of Berlin. The effects of the studied urban features on an isolated summer thunderstorm are unknown. Future research is needed to investigate the impact of isolated summer thunderstorms on urban precipitation.

The study showed a remarkable difference between the precipitation amounts in the urban areas of Berlin in case 2 and case 3. In case 2, the model simulated with the 'original' urban area of the WRF model, while in case 3 this city is replaced by an idealized circular urban area. The expectation was that the precipitation amounts in and downwind of the urban area in case 2 and 3 were almost similar because both cities had approximately the same city size. There is a slight difference in the urban temperature, but the precipitation differences in the cities and downwind area of the cities are larger (approximately 8 percent more precipitation in case 2). A good explanation for this difference in accumulated precipitation is unexpected, as the shape and the percentage land use category distribution of the two urban areas only differ slightly. In order to decrease the differences between the two urban areas, future research could execute an extra validation, to prevent large precipitation differences.

This research is mainly focused on the features of a urban area similar to Berlin (diameter of 20 [km]). However, case 3 shows that city size can affect the precipitation amounts in and downwind of a city. The different urban features for different city sizes have not examined in this research and therefore the effect is unknown. An extension of the diameters of a urban

area is needed to investigate the impact of the different urban features on convective precipitation.

The effect of the vegetation cover in the urban area was investigated in case 7. The WRF model uses land use category 5 (cropland/grassland mosaic) for the urban vegetation cover, while the rural land use category is 2 (dryland, cropland and pasture). This resulted in a small difference in urban dewpoint temperatures (0.54 [°C]). When the land use category of the urban vegetation cover is equal to 2, the values of the urban (dewpoint) temperature are closer to the temperatures in the model run without Berlin. The result is also influenced by the one urban grid cell measurement as well, which does not necessarily correspond to the situation in the entire urban area.

Finally, an additional parameter can be added in a further study on the urban precipitation, namely the 'cloud base height'. In this study, the assessment of the instability of the urban boundary is only based on the CAPE and convection. The parameter cloud base height can provide more information about the height of the urban boundary layer and consequently can provide more insight into the two mechanisms.

5   Conclusion and Recommendations

This study investigated the impact of the 'urban meteorological effect' on convective precipitation. Previous research showed mixed results on the impact of the urban area on convective precipitation. There are three main mechanisms which can cause urban precipitation disturbances: (I) low-level mechanical turbulence through urban obstructions to the airflow; (II) the addition of sensible heat flux from the urban area; (III) the urban (anthropogenic) aerosols.

This research investigated the unstable weather situation of Berlin on 11 September 2011. The first part of the study focused on an appropriate parameterization of the WRF model. To execute this part properly, different schemes of the physic and dynamic options have been evaluated.

At first, the physic and dynamic options have been validated. It was especially the start time of the model run which makes a big differences for the location of the first squall line. The validation showed that the very unstable situation was better simulated in a very short spin-up time of the model run. In this study, the start time was only six hours before the first squall line reached the urban area of Berlin.

The second part of the study investigated the impact of different urban features on the severe thunderstorm situation on 11 September 2011. Aim of the research was to understand the mechanisms of the urban impacts on regional (convective) precipitation. The focused was on the impacts of city size, anthropogenic heat, building height, albedo, vegetation factor and road width on the precipitation pattern in and around the urban area.

This study suggests approximately 0.5-4.0 [°C] higher urban temperatures and approximately 2.0 percent less to 14.7 percent more less urban precipitation in and downwind of the urban area, compared to the rural temperature and precipitation. The urban area heated up rapidly after the passage of the convergence line over the urban area, especially the urban area with high anthropogenic heats or low vegetation covers. The result indicates a decreased latent heat flux and increased sensible heat flux in the urban area, which correspond to mechanism (II). The urban vegetation cover and city size results correspond to mechanism (II) as well. The anthropogenic heats causes higher CAPE values, which results in a destabilized effect of the urban boundary layer (mechanism (I)). This results in more precipitation in the urban area as the anthropogenic heats increases. The results of the albedo and building height correspond to mechanism (I) as well.

An extra case with and without urban (anthropogenic) aerosols can be investigated in further studies, to investigate the effects of urban aerosols on convective precipitation (mechanism III). The aerosols in the urban areas can suppress and invigorate the convection and low-level convergence. Future research can focus on the amount of aerosols that determines the

suppression or invigoration of urban precipitation. Another further research can focus on the impact of a second urban area ('twin cities') on convective precipitation. The characteristics inside an urban area can differ strongly and therefore interesting to investigate the impact and interaction of the two urban areas on convective precipitation.

Acknowledgements

References

A   Internet

(1) RTL, Heftiger Regen überflutet Autobahn, retrieved from http://www.rtl.de/rtl-nachrichtenarchiv/863978/heftiger-regen-ueberflutet-autobahn.html, visited on June 21, 2013;

(2) Wetterstation Halle/Saale, Unwitter 11.9.2011, retrieved from http://wetterstationjwd.jimdo.com/unwetter-11-9-2011/, visited on June 21, 2013;

(3) Wettergefahren-Frühwarnung, Heftige Gewitter, retrieved from http://www.wettergefahren-fruehwarnung.de/Ereignis/20110913_e.html, visited on June 21, 2013;

(4) Bernard Hulsman, Het nieuwe Berlijn wordt normaal, retrieved from http://nrcboeken.vorige.nrc.nl/recensie/het-nieuwe-berlijn-wordt-normaal, visited on December 20, 2013.

B   Literature

Allen L., Lindberg F., Grimmond C.S.B., 2011: Global to city scale urban anthropogenic heat flux: model and variability. Int J Climatol. **31**, 1990-2005.

Bohnenstengel, S. I., Hamilton, I., Davies, M. and Belcher, S. E., 2013: Impact of anthropogenic heat emissions on London's temperatures. Q.J.R. Meteorol. Soc.. doi: 10.1002/qj.2144.

Bornstein R.D., 1968: Observations of the urban heat island effect in New York City. Journal of Applied Meteorology. **7**, 575-582.

Changnon S.A., Semonin R.G., Auer A.H., Braham R.R., Hales J., (1981): METROMEX: A Review and Summary. Meteorological Monograph, No. 40, American Meteorological Society: Boston, MA; 81 pp.

Changnon S.A., Shealy R.T. and Scott R.W., 1990: Precipitation Changes in Fall, Winter, and Spring Caused by St. Louis. Journal of Applied Meteorology. **30**, 126-134.

Christen A. and Vogt R., 2004: Energy and radiation balance of a central European city. Int J Climatol., **24**, 1395-1421

Collier C.G., 2006: The impact of urban areas on weather. Q.J.R. Meteorol. Soc. **132**, 1-25.

Dudhia J., 1989: Numerical study of convection observed during the winter monsoon experiment using a mesoscale two-dimensional model. J Atmos Sci., **46**, 3077-3107.

Dudhia J., 1996: A multilayer soil temperature model for MM5. Preprints, Sixth PSU/NCAR Mesoscale Model Users' Workshop, Boulder, CO, PSU/NCAR, 49-50.

Ek M.B., Mitchell K.E., Lin Y., Rogers E., Grunmann P., Koren V., Gayno G., Tarpley J.D., 2003: Implementation of the Noah land surface model advances in the National Centers for Environmental Prediction operational mesoscale Eta model. J Geophys Res., **108**, (D22), 8851, doi:10.1029/2002JD003296.2003.

Guo X., Fu D. and Wang J., 2006: Mesoscale convective precipitation system modified by urbanization in Beijing City. Atmospheric Research. **82**, 112-126.

Han J., Pan H., 2011: Revision of convection and vertical diffusion schemes in the NCEP global forecast system. Weather and Forecasting. **26**, 520-533.

Hansen, J., Public understanding of global climate change, Cambridge University Press, 282 pp., 1997.

Hong S.Y., Lim J.J., 2006: The WRF Single-Moment 6-Class Microphysics Scheme (WSM6). Journal of the Korean Meteorological Society, **42**, 129-151.

Hong S.Y., Ying N., Jimy D., 2006: A New Vertical Diffusion Package with an Explicit Treatment of Entrainment Processes. Mon Wea Rev., **134**, 2318-2341.

Huff F.A. and Changnon S.A., 1973: Precipitation modification by major urban areas. Illinois State Water Survey. **54**, 1220-1232.

Janjic Z.I., 2002: Nonsingular implementation of the Mellor-Yamada level 2.5 scheme in the NCEP Meso model. NCEP Office Note 437, National Centers for Environmental Prediction, 61 pp.

Jin M., Shepherd J.M., King M.D., 2005: Urban aerosols and their variation with clouds and rainfall: A case study for New York and Houston. Journal of Geophysical Research. 110, doi:10.1029/2004JD005081.

Kain J.S., Fritsch J.M., 1993: Convective parameterization for mesoscale models: The Kain-Fritsch scheme. Meteorological Monographs, **24**, 165-170.

Lin C., Chang, P. and Sheng, Y., 2011: Impact of the Urban Heat Island Effect on Precipitation over a Complex Geographic Environment in Northern Taiwan. J. Appl. Meteor. Climatol. **50**, 339-353.

Jauregui E. and Romales E., 1996: Urban effects on convective precipitation in Mexico City. Atmospheric Environments. **30**, 3383-3389.

Kondo H., 2012: Modification of MUCM to include water cycle under rainy weather conditions. ICUC8 – 8th International Conference on Urban Climates, Dublin.

Matheson M.A. and Ashie Y., 2008: The Effect of Changes of Urban Surfaces on Rainfall Phenomenon as Determined by a Non-Hydrostatic Mesoscale Model. Journal of the Meteorological Society of Japan. **86**, 733–751.

Mellor G.L., Yamada T., 1982: Development of a turbulence closure model for geophysical fluid problems. Rev Geophys Space Phys., **20**, 851–875.

Miao S., Chen F., Li Q. and Fan S., 2010: Impacts of Urban Processes and Urbanization on Summer Precipitation: A Case Study of Heavy Rainfall in Beijing on 1 August 2006. Journal of Applied Meteorology and Cliatology. **50**, 806–825.

Mlawer, E. J., Taubman S. J., Brown P. D., Iacono M. J., 1997: Radiative transfer for inhomogeneous atmospheres: RRTM, a validated correlated-k Model for the longwave. J. Geophys. Res. **102**, 16663–16682.

Oke T.R., 1982: The energetic basis of the urban heat island. Quarterly Journal of the Royal Meteorological Society. **108**, 1–24.

Oke, T.R., 2006: Towards better scientific communication in urban climate. Theor. Appl. Climatol. **84**, 179–190;

Pagowski M., 2004: Some Comments on PBL Parameterizations in WRF. NOAA Research-Forecast System Laboratory, The Joint WRF/MM5 Users' Workshop.

Ramanathan V., Crutzen P.J., Kiehl J.T., Rosenfeld D., 2001: Aerosols, Climate, and the Hydrological Cycle. Science. **294**, 2119–2124.

Rogers, E., and Coauthors, 2009: The NCEP North American Mesoscale modeling system: Recent changes and future plans. Preprints, 23rd Conf. on Weather Analysis and Forecasting/19th Conf. on Numerical Weather Prediction, Omaha, NE, Amer. Meteor. Soc., 2A4.

Schmid, P.E. and Niyogi, D., 2013: Impact of City Size on Precipitation-Modifying Potential. Geophysical Research Letters. DOI: 10.1002/grl.50656.

Seino N. and Aoyagi T., 2012: Impact of urbanization on precipitation in the Tokyo area. Numerical simulation for summer cases. ICUC8 – 8th International Conference on Urban Climates, Dublin.

Shem W., Shepherd, M., 2008: On the impact of urbanization on summertime thunderstorms in Atlanta: Two numerical model case studies. Atmospheric Research. **92**, 172-189.

Skamarock W.C., Klemp J.B., Dudhia J., Gill D.O., Barker D.M., Duda M.G., Huang X.Y., Wang W., Powers W.G., 2008: A Discripion of the Advanced Research WRF Version 3, NCAR technical note, Boulder, USA.

Stepherds, J.M. and Burian, S.J., 2003: Detection of Urban-Induced Rainfall Anomalies in a Major Coastal City. Earth Interactions. **7**, 1-17.

Taha, H., 1997: Urban climates and heat islands: albedo, evapotranspiration, and anthropogenic heat. Energy and Buildings, **25**, 99-103.

Tayanç M., Karaca M., Yenigün O., 1997: Annual and seasonal air temperature trend patterns of climate change and urbanization effects in relation to air pollutants in Turkey. J Geophys Res. **102**, 1909-1919.

Theeuwes, N.E., Steeneveld G.J., Ronda R.J., Heusinkveld B.G., Holtslag A.A.M., 2012: Mitigation of the urban heat island effect using vegetation and water bodies. 8th International Conference on Urban Climates, 6th-10th August, 2012, UCD, Dublin Ireland.

Theeuwes N. E., Solcerová A., Steeneveld G.J., 2013: Modeling the influence of open water surfaces on the summertime temperature and thermal comfort in the city, J. Geophys. Res. Atmos.,**118**, 8881-8896, doi:10.1002/jgrd.50704.

United Nations Population Fund, 2007: State of world population 2007, Unleashing the potential of urban growth. Retrieved from http://www.unfpa.org/public/publications.

Wan H., Zhong Z., Yang X. and Li X., 2012: Ensembles to model the impact of urbanization for a summertime rainstorm process in Yangtze River Delta, China. Meteorological Applications. Doi: 10.1002/met.1360.

Wan H., Zhong Z., 2013: Ensemble simulations to investigate the impact of large-scale urbanization on precipitation in the lower reaches of Yangtze River Valley, China. Q. J. R. Meteorol. Soc. DOI:10.1002/qj.2125

Willems P., Arnbjerg-Nielsen K., Olsson J. and Nguygen V.T.V., 2012: Climate change impact assessment on urban rainfall extremes and urban drainage: Methods and shortcomings. Atmospheric Research. **103**, 106-118.
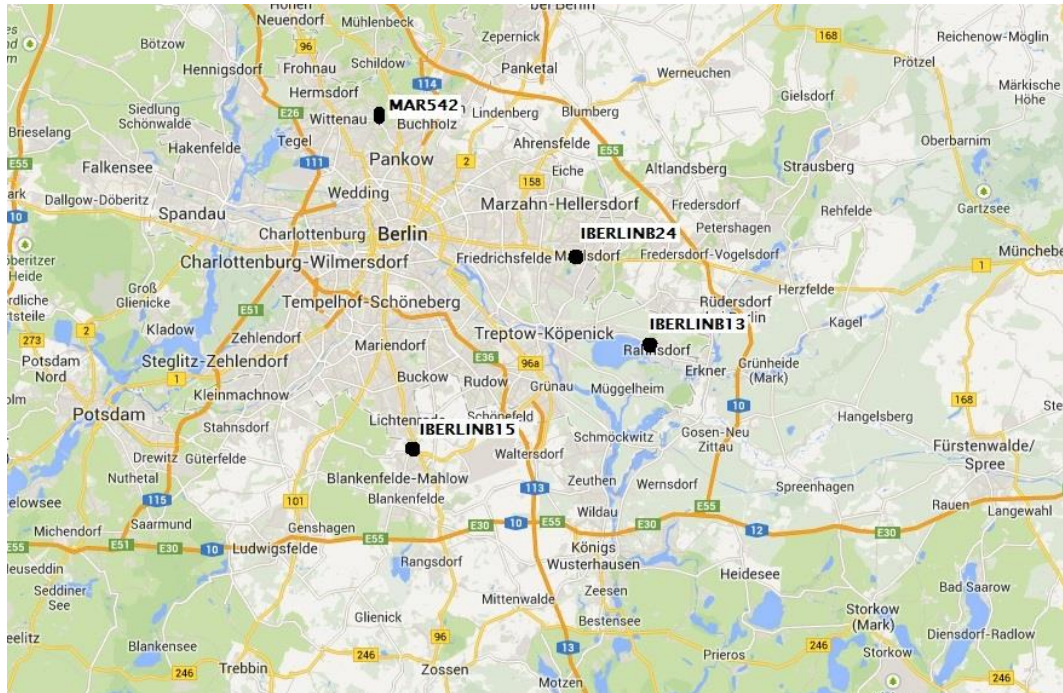
Willmott C.J., 1982: Some Comments on the Evaluation of Model Performance. Bulletin American Meteorological Society. **63**, 1309-1313.

Yang L., Tian F., Smith J.A., Hu H., 2014: Urban Signatures in the Spatial Clustering of Summer Heavy Rainfall Events over the Beijing Metropolitan Region. Journal of Geophysical Research-Atmosphere. Doi: 10.1002/2013JD020762.
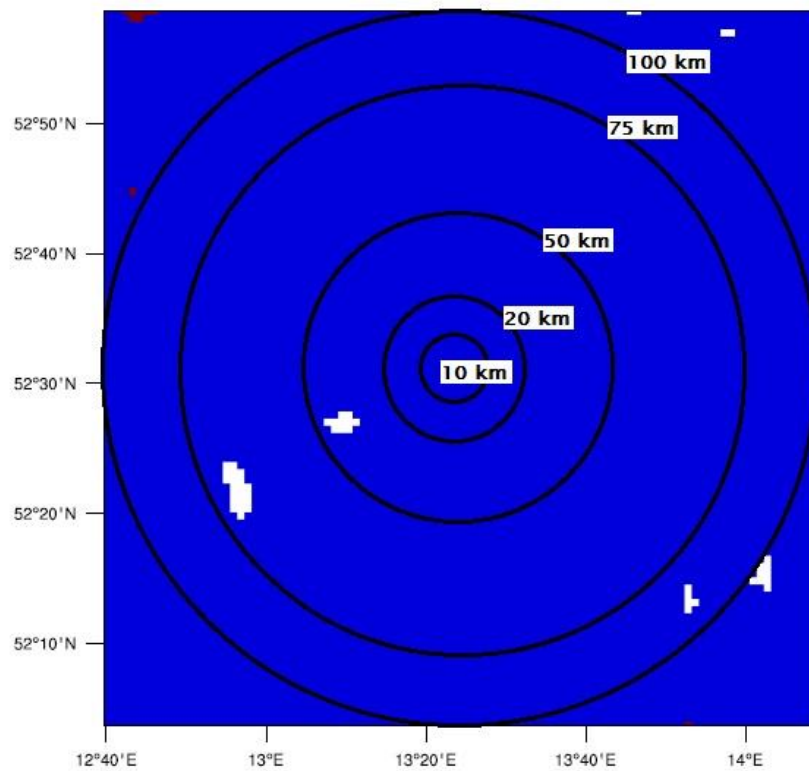
Yair, Y., Lynn B., Price C., Kotroni V., Lagouvardos K., Morin E., Mugnai A., and Llasat M.C., 2010: Predicting the potential for lightning activity in Mediterranean storms based on the Weather Research and Forecasting (WRF) model dynamic and microphysical fields, J. Geophys. Res., 115, doi:10.1029/2008JD010868.

Zhang, K., Wang R., Shan, C., & Da, L., 2009: Temporal and spatial characteristics of the urban heat island during rapid urbanization in Shanghai, China. Environmental Monitoring and Assessment. 169, (1-4), 101-112.
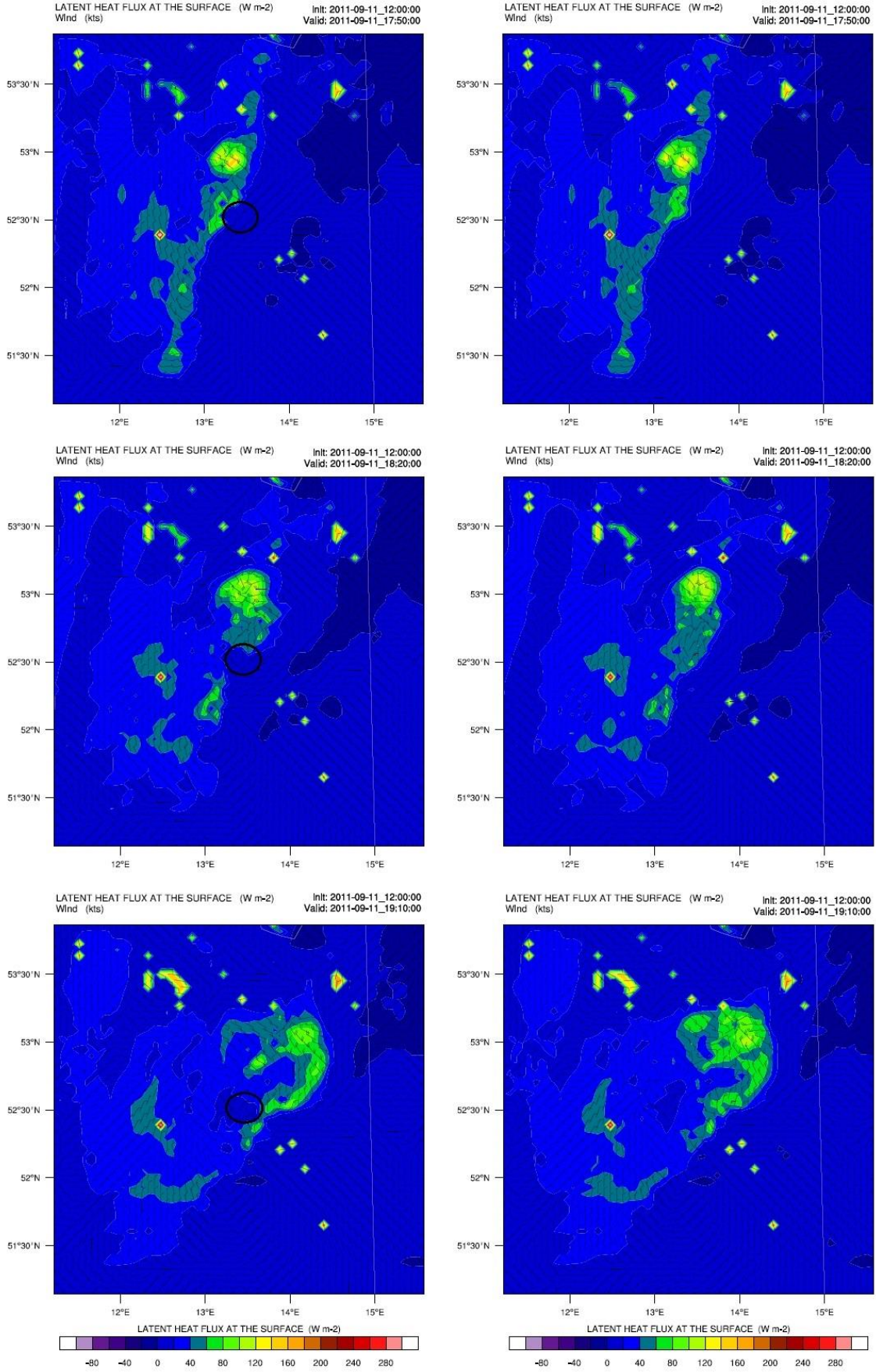
Annex

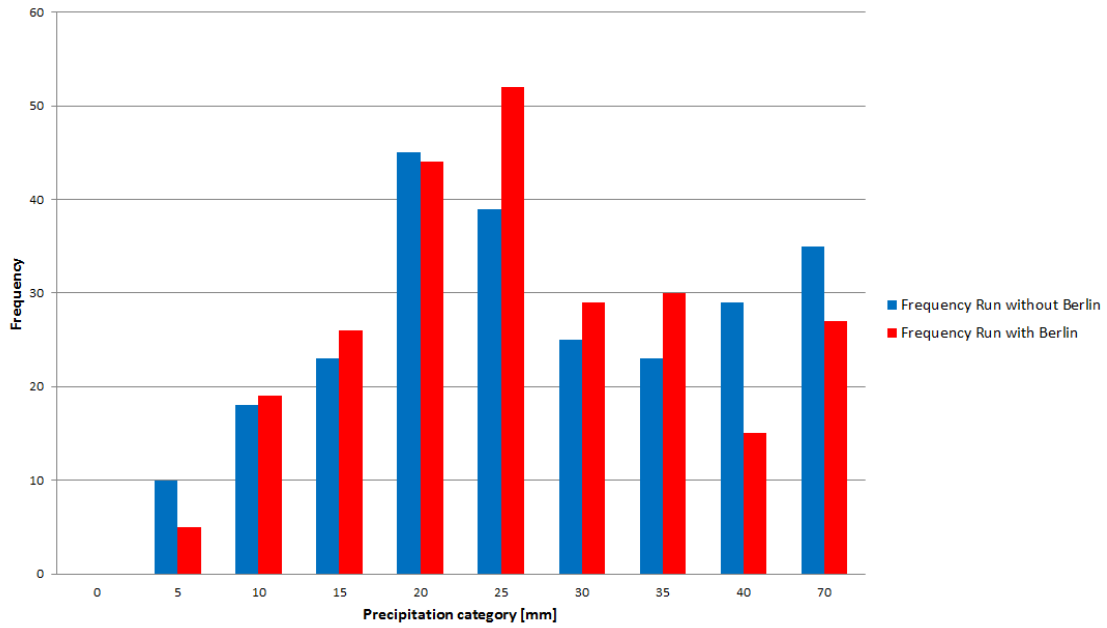*Figure 21.* The location of the four Wunderground weather station in the urban area of Berlin.

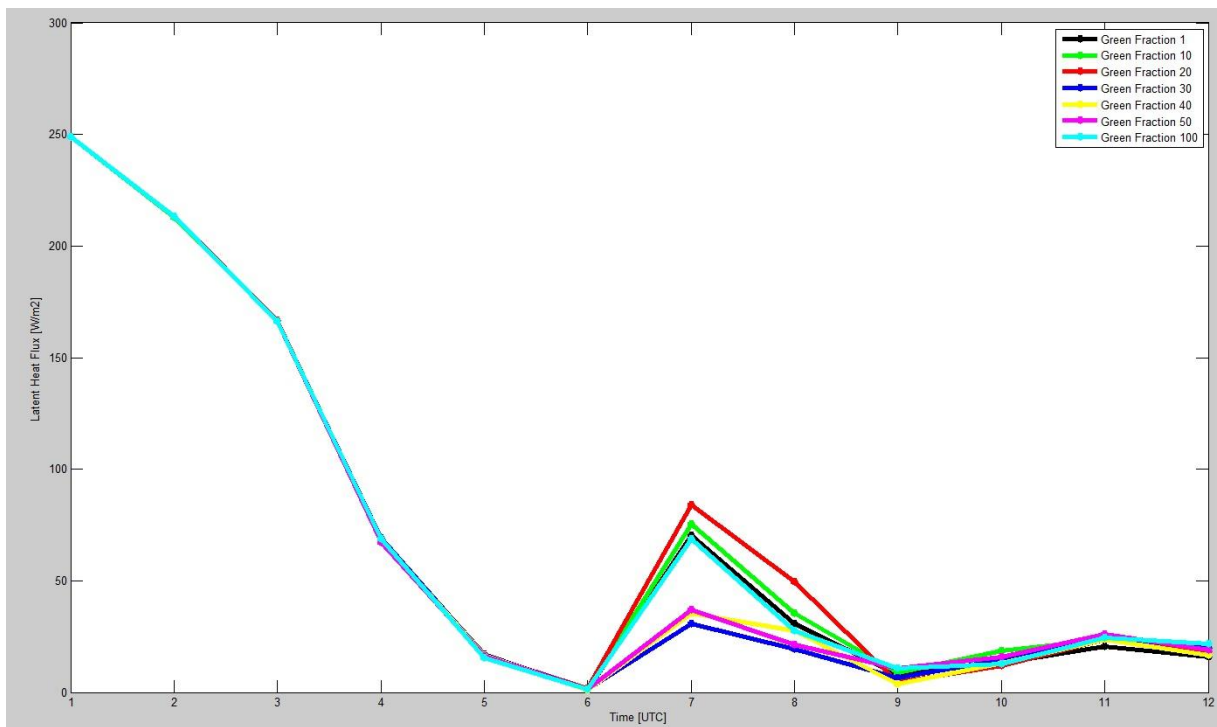*Figure 22.* The different urban area sizes used in case 3.

Figure 23. The latent heat flux in domain 3 with Berlin (left hand side) and without Berlin (right hand side).

Figure 24. *The sensible heat flux in domain 3 with Berlin (left hand side) and without Berlin (right hand side).*
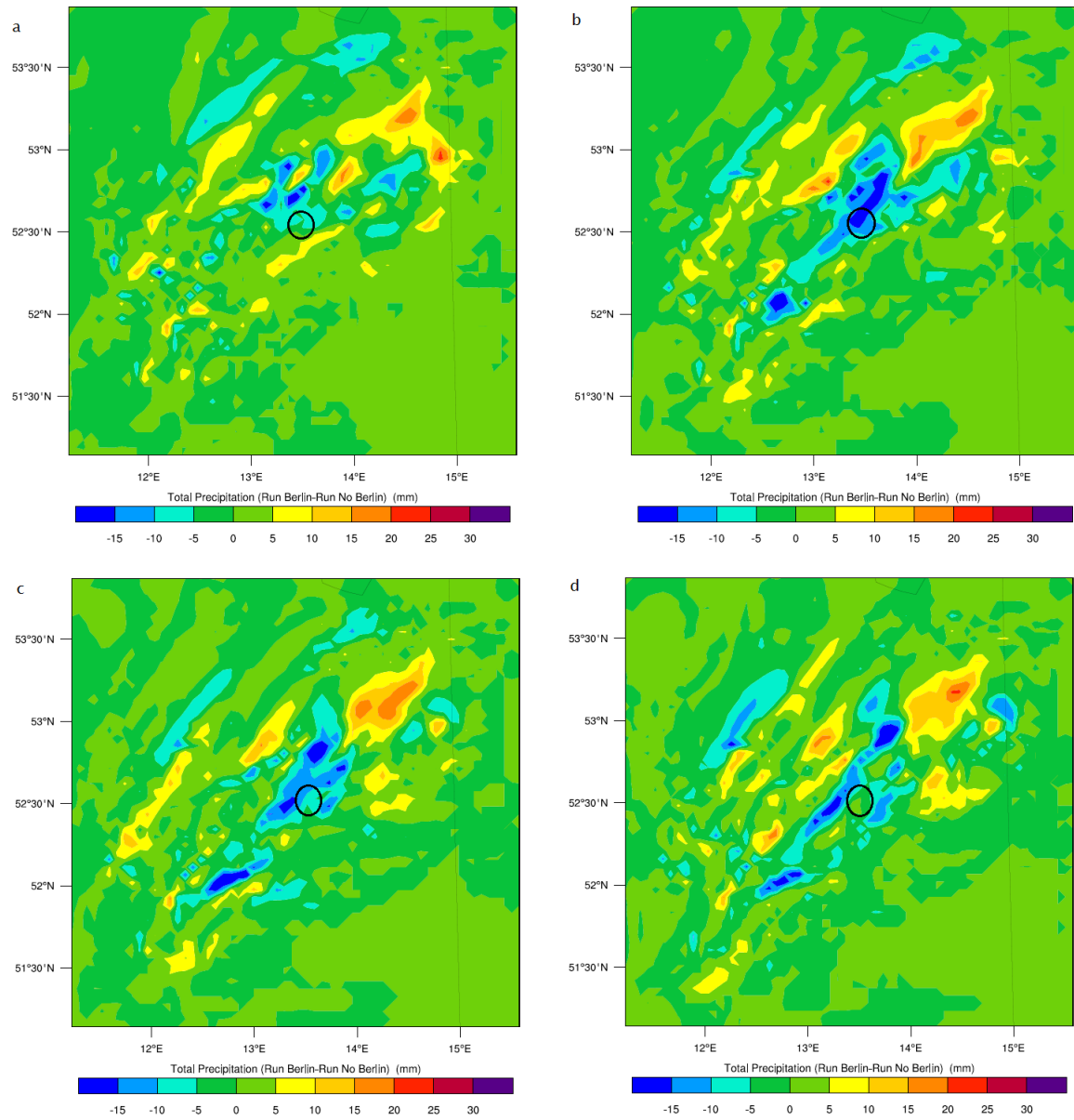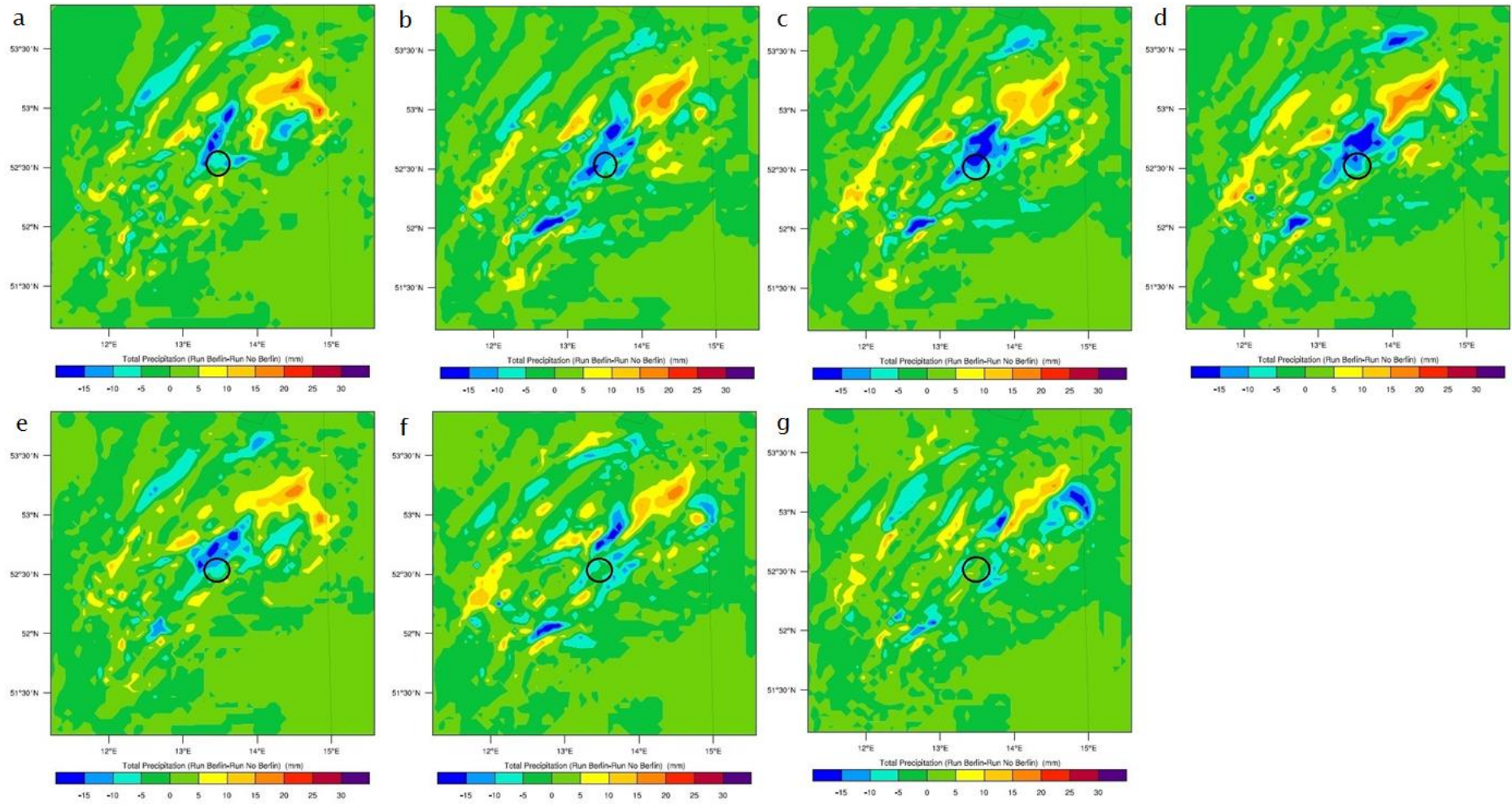
Figure 25. *Histogram with the precipitation distribution in the area downwind of Berlin in the model run without Berlin (blue bars) and the precipitation distribution in the model run with Berlin (red bars).*

Figure 26. *The latent heat fluxes plotted against the time for the urban area with difference vegetation fractions (Case 7). In the situation of the first squall line, the latent heat fluxes showed a dichotomy. The vegetation fraction 30, 40 and 50 percent showed lower latent heat fluxes compared to the remaining model runs.*

Figure 27. *The precipitation difference with different albedo's in domain 2, a) an albedo of 0.1, b) albedo of 0.15, c) albedo of 0.2 and d) an albedo of 0.3.*

Figure 28. The precipitation difference between the urban area with different vegetation fractions and the rural area in domain 2. The vegetation fractions have been a) 1 percent, b) 10 percent, c) 20 percent, d) 30 percent, e) 40 percent, f) 50 percent and g) 100 percent in the urban area.